Evidence of Carboniferous Arc Magmatism Preserved in the Chicxulub Impact Structure

Catherine H. Ross[1,2,*], Daniel F. Stockli[1], Cornelia Rasmussen[1,2], Sean P.S. Gulick[1,2,3], Sietze J. de Graaff[4,5], Philippe Claeys[4], Jiawei Zhao[6], Long Xiao[6,7], Annemarie E. Pickersgill[8,9], Martin Schmieder[10], David A. Kring[10], Axel Wittmann[11], Joanna V. Morgan[12]

**Corresponding author, Email: catherine.ross@utexas.edu (Catherine H. Ross),*

[1]Dept. of Geological Sciences, Jackson School of Geosciences, University of Texas at Austin, 22275 Speedway Stop C9000 Austin, TX 78712 USA

[2]Institute for Geophysics, J.J. Pickle Research Campus, Building ROC, University of Texas at Austin, 10100 Burnet Road (R2200) Austin, TX USA

[3]Center for Planetary Systems Habitability, University of Texas at Austin, Austin, Texas, USA

[4]Research Unit: Analytical, Environmental and Geo-Chemistry, Department of Chemistry, Vrije Universiteit Brussel, AMGC-WE-VUB, Pleinlaan 2, 1050 Brussels, Belgium. sietze.de.graaff@vub.be, phclaeys@vub.be

[5]Laboratoire G-Time, Université Libre de Bruxelles, Av. F.D. Roosevelt 50, 1050 Brussels, Belgium.

[6]State Key Laboratory of Geological Processes and Mineral Resources, Planetary Science Institute, School of Earth Sciences, China University of Geosciences, Wuhan, China

[7]State Key Laboratory of Space Science Institute, Lunar and Planetary Science, Macau University of Science and Technology, Taipa, Macau, China

[8]School of Geographical and Earth Sciences, University of Glasgow, Glasgow, U.K.

[9]NERC Argon Isotope Facility, Scottish Universities Environmental Research Centre (SUERC), Glasgow, UK
[10]Center for Lunar Science and Exploration, Lunar and Planetary Institute, Houston, TX
[11]Eyring Materials Center, Arizona State University Tempe, AZ
[12]Department of Earth Science and Engineering, Imperial College London, UK

ABSTRACT

Determining the nature and age of the 200-km-wide Chicxulub impact target rock is an essential step in advancing our understanding of the Maya Block basement. Few age constraints exist for the northern Maya Block crust, specifically the basement underlying the 66 Ma, 200 km-wide Chicxulub impact structure. The International Ocean Discovery Program-International Continental Scientific Drilling Program Expedition 364 core recovered a continuous section of basement rocks from the Chicxulub target rocks, which provides a unique opportunity to illuminate the pre-impact tectonic evolution of a terrane key to the development of the Gulf of Mexico. Sparse published ages for the Maya Block point to Mesoproterozoic, Ediacaran, Ordovician to Devonian crust are consistent with plate reconstruction models. In contrast, granitic basement recovered from the Chicxulub peak ring during Expedition 364 yielded new zircon U-Pb laser ablation-inductively coupled plasma-mass spectrometry (LA-ICP-MS) concordant dates clustering around 334 ± 2.3 Ma. Zircon rare earth element (REE) chemistry is consistent with the granitoids having formed in a continental arc setting. Inherited zircon grains fall into three groups: 400–435 Ma, 500–635 Ma, and 940–1400 Ma, which are consistent with the incorporation of Peri-Gondwanan, Pan-African, and Grenvillian crust, respectively. Carboniferous U-Pb ages, trace element compositions, and inherited zircon grains indicate a pre-collisional continental volcanic arc located along the Maya Block's northern margin before NW

Gondwana collided with Laurentia. The existence of a continental arc along NW Gondwana suggests southward-directed subduction of Rheic oceanic crust beneath the Maya Block and is similar to evidence for a continental arc along the northern margin of Gondwana that is documented in the Suwannee terrane, Florida, USA, and Coahuila Block of NE México.

INTRODUCTION

The Chicxulub structure is the largest known Phanerozoic impact structure and has been linked to the Cretaceous-Paleogene (K-Pg) extinction event and boundary sections through geochemistry, geochronology, and proximal deposit thicknesses (e.g., Hildebrand et al., 1991; Kring and Boynton, 1992; Swisher et al., 1992; Krogh et al., 1993a, 1993b; Kamo and Krogh, 1995; Kring, 1995; Schulte et al., 2010; Kamo et al., 2011). The ~200-km-diameter structure was formed when a 12 km bolide impacted the Yucatán Peninsula in México from the NNE (Gulick et al., 2008; Collins et al., 2020). A positive iridium anomaly represents the original connection between the K-Pg mass extinction and an extraterrestrial source (Alvarez et al., 1980; Ganapathy, 1980; Kyte et al., 1980; Smit and Hertogen, 1980). Since that discovery, numerous geological and geophysical studies have been conducted of the Chicxulub impact structure and its related hydrothermal system, associated ejecta, tsunami deposits, as well as its climatic and biological effects (e.g., Smit, 1999; Kring, 2005; Schulte et al., 2010; Gulick et al., 2019). The Chicxulub target rock sequence is heterogeneous and is comprised of ~3 km of Jurassic-Cretaceous sedimentary packages of limestone, dolomite, marl, and anhydrite (Kring, 2005). The underlying basement of the Chicxulub crater is predominantly composed of granitoids, amphibolite, dolerite, and ortho- and paragneiss (Kring, 2005; Keppie et al., 2011; Morgan et al., 2016; de Graaff et al., 2021). However, exposures or drill core recoveries of the northern Maya

Block basement are rare, and its tectono-magmatic evolution remains highly incomplete with fundamental questions about the Phanerozoic tectonic evolution lingering.

Crustal blocks such as Maya, Oaxaquia, Mérida Andes, Chortís, and Coahuila were separated from the western margin of Gondwana in the early Paleozoic and subsequently incorporated into Paleozoic collisional orogens (Nance et al., 2008). These terranes are commonly referred to as "Peri-Gondwanan" terranes. The Chortís Block is a terrane in Central America (Honduras, Nicaragua, El Salvador, Guatemala, and off-shore Nicaragua Rise) located to the south of the Maya Block and separated from it by the Motagua-Polochic Fault Zone (e.g., Ratschbacher et al., 2009). The Mérida Andes of western Venezuela record early Paleozoic and early Mesozoic collisional and extensional tectonic events, respectively (Tazzo-Rangel et al., 2020). The tectonic backbone of México is composed of granulite-facies Mesoproterozoic basement, which constitutes an terrane known as Oaxaquia (e.g., Ortega-Gutierrez et al., 1995). The Coahuila Block of northeastern México lies south of the Ouachita suture and represents a fragment of Peri-Gondwanan crust that has not been displaced significantly since juxtaposition with Laurentia in Pangea (Dickinson and Lawton, 2001).

Since the first reconstructions, the paleogeographic positions and tectonic interactions of pre-Mesozoic crustal blocks in México, Central America, and the Caribbean region have been debated (Bullard et al., 1965; Pindell and Dewey, 1982; Ross and Scotese, 1988; Marton and Buffler, 1994; Pindell et al., 2000; Dickinson and Lawton, 2001; Mann et al., 2007). The rifting of Laurentia (present-day North America) away from Gondwana (present-day South America and Africa) marks Paleozoic plate kinematics. The Rheic Ocean separated these plates beginning in the Early Ordovician and subsequently closed during the formation of supercontinent Pangea due to the Pennsylvanian collision of Gondwana and Laurentia (e.g., Nance and Linnemann, 2008). Documenting the pre-Mesozoic position of the Maya Block and its relationship to the SW Laurentian margin is essential to complete plate reconstructions of the final assembly of Pangea as well as the Jurassic Gulf of Mexico rifting and opening due to rotation. Models have placed the Maya Block in different locations and various orientations at the end of the Paleozoic and the early Mesozoic (e.g., Pindell and Dewey, 1982; Dickinson and Lawton, 2001; Steiner, 2005; Mann et al., 2007; Stern and Dickinson, 2010). The tectono-magmatic history of the Maya Block and in particular constraining the location, timing, and subduction polarity of the late Paleozoic magmatic arc related to Rheic Ocean closure is vital for understanding both the formation and breakup of Pangea along the SW margin of Laurentia and NW margin of Gondwana.

Due to the extensive Mesozoic sedimentary cover and a rarity of deep boreholes, Maya Block pre-Mesozoic rocks are only exposed in Mixtequita (Guichicovi Complex), the Chiapas Massif, central Guatemala, the Maya Mountains in Belize, and ejecta/breccia clasts from the Chicxulub impact structure. These studies focused on granitic and metamorphic clasts from impact breccias and suevites within the Chicxulub impact structure or proximal sites in México (Krogh et al., 1993a, 1993b; Kamo and Krogh, 1995; Kettrup and Deutsch, 2003; Keppie et al., 2011; Schmieder et al., 2018; Zhao et al., 2020). Additional age constraints derive from studies of Chicxulub distal K-Pg ejecta material in Spain, Colorado, Saskatchewan, and Haiti (Krogh et al., 1993a, 1993b; Kamo and Krogh, 1995; Kamo et al., 2011). The uplift of mid- to upper-crustal granitic basement blocks through cratering processes preserved within the International Ocean Discovery Program-International Continental Scientific Drilling Program (IODP-ICDP)

Expedition 364 core (Hole M0077A; 21.45°N, 89.95°W) provides a new opportunity to better constrain the pre-impact tectonic evolution of the Maya Block. An initial U-Pb study of 40 zircon grains from five basement samples recovered at Site M0077 was presented in Zhao et al. (2020). In contrast to Zhao et al. (2020), who used conventional laser ablation-inductively coupled plasma-mass spectrometry (LA-ICP-MS) analysis on polished internal zircon surfaces, this study employed depth profile analysis of unpolished zircon grains. Our detailed study described here of the zircon U-Pb geochronology and trace element signatures of the Chicxulub peak ring builds on recent work with IODP-ICDP Expedition 364 samples (e.g., Schmieder et al., 2017; Rasmussen et al., 2019; Zhao et al., 2020; Timms et al., 2020).

These new data constrain the tectonic setting and location of the Maya Block in the Late Paleozoic, which has significant implications for its tectonic reconstruction prior to and during the opening of the Gulf of Mexico. While Carboniferous U-Pb ages were recovered from within the crater itself (drill sites Yucatán-6 and Yaxcopoil-1) as well as from both proximal and distal K-Pg deposits (Haiti, Colorado, Saskatchewan, and Spain), these ages were not considered to be an important fingerprint of the Chicxulub target lithologies or the Maya Block (Krogh et al., 1993a, 1993b; Kamo and Krogh, 1995; Kamo et al., 2011; Keppie et al., 2011; Schmieder et al., 2017, 2018). The origin of these Carboniferous ages was hypothesized to be Maya Block continental arc rocks, with no elaboration about the tectonic significance or if the Pb-loss ages along a discordia trajectory between the Pan-African (550 Ma) and the K-Pg impact event at 66 Ma (Kamo et al., 2011).

Geochronologic results from basement rock of the Chicxulub impact structure represent a critical step in understanding the composition of the target material, the post-impact hydrothermal system, and proximal and distal ejecta deposits. Ejecta atmospheric dispersion reconstructions and climate models currently rely on ejecta distribution thickness and composition and include quantification of the Ir anomalies (Alvarez, 1996; Claeys et al., 2002; Collins, 2002; Kring and Durda, 2002; Collins et al., 2008; Artemieva and Morgan, 2009; Artemieva and Morgan, 2020). However, these models can be improved through a more comprehensive understanding of the Maya Block's age signature preserved within the Chicxulub impact structure. Identifying source rocks in ejecta components in K-Pg boundary deposits may allow for better tracking of global ejecta dispersal and composition. A better Chicxulub basement age signature makes it possible to estimate the relative volumes of different basement materials ejected from the crater.

GEOLOGIC SETTING

The pre-Mesozoic tectonic and magmatic evolution of the Maya Block and, specifically, its northern portion, is poorly constrained due to the very sparse and geographically limited Paleozoic and Precambrian outcrops as well as the extensive Mesozoic and Cenozoic sedimentary cover (Lopez Ramos, 1975). The crustal backbone of central, eastern, and southern México is formed by late Mesoproterozoic protoliths (1.25–1.0 Ga) with granulite facies metamorphism (ca. 0.99 Ga) making up the Oaxaquia microcontinent (e.g., Ortega-Gutiérrez et al., 1995, 2018; Fig. 1A). Emplacement of Ediacaran rift-related mafic dyke swarms and deposition of metasedimentary units occurred in NE México and Chiapas during the final fragmentation of Rodinia and opening of the Iapetus Ocean (González-Guzmán et al., 2016; Weber et al., 2019, 2020). Ordovician (ca. 480–450 Ma) magmatism and crustal anatexis, as recorded in Chiapas, Altos Cuchumatanes, and Rabinal, suggest that these terranes likely formed the northern continuation of the Famatinian arc along the western margin of Gondwana (Estrada-Carmona et al., 2012; Weber et al., 2018; Alemán-Gallardo et al., 2019; Ortega-Obregón et al., 2008, 2009; Juárez-Zúñiga et al., 2019).

By the Devonian, the Rheic Ocean was closing, ultimately leading to the complete subduction of its oceanic crust and the formation of the Pangean supercontinent in the late Paleozoic, which resulted in deformation and tectonic reorganization of the Mexican terranes (e.g., Nance et al., 2007). Along the NW margin of Gondwana, this convergence culminated in a laterally diachronous collision and suturing of Gondwana and associated terranes with Laurentia during the Ouachita-Marathon-Appalachian orogeny in the latest Carboniferous and Early Permian (e.g., Dickinson and Lawton, 2001). In paleotectonic models, it has been suggested that the Maya Block: (1) has a pre-Mesozoic Gondwanan affinity (e.g., Pindell et al., 1988; Pindell and Kennan, 2009; Weber et al., 2009); (2) is a peri-Gondwanan, arc-related terrane formed either before the opening of the Iapetus Ocean (Keppie et al., 2011); or more controversially (3) is a rifted Laurentian basement block (Keppie and Keppie, 2014). In particular, the nature and origin of the latest Neoproterozoic magmatism remain unclear and could be associated with Peri-Gondwanan subduction, the Brasiliano (Pan-African) orogeny, or late-stage Cadomian magmatism (e.g., Ortega-Gutiérrez et al., 2018). Hence, new age determinations for the Maya Block basement and comparison with ages of surrounding Laurentian and Gondwanan terranes provide new insights into constraints on the Neoproterozoic and Phanerozoic paleogeographic and tectonic evolution before the opening and subsequent closure of the Rheic Ocean, including subduction zone polarity as well as Mesozoic reconstructions of the later Gulf of Mexico opening.

Oaxaquia terrane

Oaxaquia is part of the Grenville orogenic belts that are associated with the amalgamation of the Mesoproterozoic supercontinent Rodinia (1.1–1.0 Ga; Dalziel, 1997). There are only a few exposures of the late Mesoproterozoic Oaxaquian basement including the Novillo Gneiss (Fig. 1; Keppie et al., 2003; Cameron et al., 2004; Trainor et al., 2011; Weber et al., 2019), the Huiznopala Gneiss (Lawlor et al., 1999; Weber and Schulze, 2014), the Oaxacan Complex (Keppie et al., 2003; Solari et al., 2003, 2004a, 2004b), and the Guichicovi Complex (Weber and Köhler, 1999; Weber and Hecht, 2003). Pre-Mesozoic rocks of the Guichicovi Complex are characterized by 1.2 Ga igneous, arc-related protoliths and ca. 1.02–1.01 Ga anorthosite-mangerite-charnockite granites that were metamorphosed under granulite facies conditions between 990 Ma and 975 Ma (Weber and Köhler, 1999; Ruiz et al., 1999; Weber et al., 2010). The Guichicovi Complex also records another Tonian metamorphic event from Sm-Nd garnet-whole rock dates of 933 ± 6 Ma and 911 ± 12 Ma (Weber and Köhler, 1999). The $T_{DM(Nd)}$ (depleted mantle) model ages are 1.35–1.63 Ga and 1.52–2.02 Ga for the meta-igneous and sedimentary rocks, respectively (Weber and Köhler, 1999). The Oaxaquia backbone appears to have formed as juvenile arc crust off Amazonia in the early Mesoproterozoic, matured around 1.2 Ga, and experienced subsequent deformation and high-grade metamorphism during an arc-continental and continent-continent collision with Avalonia and/or Baltica in the earliest Neoproterozoic (e.g., Keppie and Dostal, 2007; Keppie and Ortega-Gutiérrez, 2010; Weber et al., 2010; Weber and Köhler, 1999; Weber and Schulze, 2014).

Maya Block

The Maya Block is widely viewed as a peri-Gondwanan terrane that forms the pre-Mesozoic basement of Yucatán Peninsula, its Gulf of Mexico shelf, Chiapas, and north-central Guatemala (Weber et al., 2009; Keppie et al., 2010; Martens et al., 2010; Fig. 1). It is separated from the Chortís Block of Central America by the Motagua-Polochic Fault system. While the northern Maya Block (underlying the Chicxulub crater) appears to be principally ca. 550 Ma Pan-African basement (Krogh et al., 1993a, 1993b; Keppie et al., 2011), no such basement has been described from the southern Maya Block near Chiapas. Early Paleozoic sandstone from the southern Maya Block are mainly devoid of Pan-African detrital zircon in Belize but are present in the Santa Rosa Formation exposed in the Chiapas Massif Complex (Martens et al., 2010; Weber et al., 2008; González-Guzmán, 2016). In contrast, the southern Maya Block is dominated by Permian igneous and metamorphic rocks (Schaaf et al., 2002; Weber et al., 2005, 2007). Ordovician-Devonian igneous and meta-sedimentary rocks only occur in the El Triunfo Complex of the southeasternmost Chiapas Massif Complex (Estrada-Carmona et al., 2012; Weber et al., 2018). This Ordovician magmatism was likely associated with Ordovician Famatinian arc magmatic activity stretching from South America to northern Central America (Estrada-Carmona et al., 2012; Alemán-Gallardo et al., 2019).

The geological reconstruction of the Maya Block basement has been hampered by both the lack of continuous exposures and age constraints as well as its Mesozoic dismemberment during the Gulf of Mexico opening, which includes substantial translation of the block along the East México or Tehuantepec transform fault system (e.g., Pindell, 1985; Pindell et al., 2020). These reconstructions point to a connection of the Maya Block with the basement of NE México prior to the opening of the Gulf of Mexico (e.g., Alemán-Gallardo et al., 2019), where the area west of the East Mexican transform in NE México is composed of Peri-Gondwanan basement intruded by Ordovician plutons. The following sections summarize basement rocks and ages that are exposed in the region.

Maya Mountains (Belize)

The basement of the Maya Mountains in central Belize is composed of diorite, granodiorite, and granite with Silurian intrusive U-Pb ages of 420–405 Ma with an inherited age component of 1210 ± 136 Ma (Fig. 1; Steiner and Walker, 1996). Metasedimentary detrital zircon source components include late Mesoproterozoic to early Neoproterozoic (1.2–0.9 Ga) and minor early Mesoproterozoic (1.6–1.4 Ga) and are intruded by Late Silurian to Early Devonian (ca. 415–400 Ma) granitoids (Weber et al., 2012). Late Triassic K-Ar ages from these plutons (ca. 237–205 Ma) were first interpreted as the intrusion age (Bateson and Hall, 1977; Dawe, 1984) but were then considered cooling ages related to Pangea breakup in light of the Silurian U-Pb ages. The basement is overlain by rhyolite interbedded with conglomerates; these rhyolites yielded a U-Pb date of 406 + 7/–6 Ma (Martens et al., 2010). This Silurian magmatic activity is likely linked to a subduction-related tectonic setting due to the rotation in plate motion direction of the northern Rheic Ocean (Weber et al., 2012).

Altos Cuchumatanes and Rabinal

Maya Block crystalline basement is exposed north of the Polochic Fault Zone in the Altos Cuchumatanes of Guatemala, where magmatism occurred during the Middle Ordovician (461 Ma) with granodiorite intruding into ca. 1 Ga medium- to high-grade gneiss. This Ordovician magmatism likely occurred in a convergent tectonic setting possibly linked to the Famatinian arc (Solari et al., 2010; Juárez-Zúñiga et al., 2019; Weber et al., 2018). Magmatism also occurred in the lower Pennsylvanian (312–317 Ma) due to an east-dipping subduction zone that accommodated convergence between Laurentia and Gondwana (Solari et al., 2010). The Rabinal granite in central Guatemala, which intruded into metasedimentary rocks of the San Gabriel sequence at 462–445 Ma, is older than nearby plutons in the Maya Mountains (Solari et al., 2013). These dates are similar to the ca. 480–440 Ma magmatic ages in the Acatlán Complex of southern México (e.g., Miller et al., 2007) and ages in the Motozintla area of Chiapas (Estrada-Carmona et al., 2012).

Chiapas Massif Complex

The Chiapas Massif Complex is a large NW-SE elongated crystalline belt in SE México, which parallels the Pacific coast and is mainly composed of the relatively undeformed Permian Chiapas batholith (Fig. 1; Schaaf et al., 2002; Weber et al., 2005, 2007). Similar to cooling ages in the Guichicovi Complex, Tonian metamorphism is recorded by zircon U-Pb ages from the southern Chiapas Massif Complex (El Triunfo Complex), such as the 919 ± 13 Ma Chipilin Gneiss (Weber et al., 2018). However, the massif also contains pre-Permian metamorphic basement rocks composed of orthogneisses, anatexites, and amphibolites intruded by Ordovician granites and then by the Late Permian batholith (Schaaf et al., 2002; Estrada-Carmona et al., 2012; Weber et al., 2018). The Late Permian batholith rocks range in age from 270 Ma to 250 Ma. Permian zircon grains from the batholith exhibit inherited ca. 1 Ga cores. Similarly, the $T_{DM(Nd)}$ model ages range from 1.0 Ga to 1.4 Ga (Schaaf et al., 2002). There are ca. 1 Ga gneisses and anorthosites exposed within the southern Chiapas Massif (Cisneros de León et al., 2017; Weber et al., 2018). These exposures, model ages, and inherited zircon cores suggest that the ca. 1 Ga Oaxaquia basement underlies the Chiapas Massif. The Ordovician granites also suggest a genetic link between Chiapas, Rabinal, Altos Cuchumatanes, and the Maya Mountains.

Southeast Gulf of Mexico

On the Yucatán Platform, NE of the Yucatán Peninsula and SW of Florida, Deep Sea Drilling Project (DSDP) Sites 537 and 538A recovered gneiss, amphibolite, and phyllite samples that recorded Ordovician (ca. 500 Ma) $^{40}Ar/^{39}Ar$ ages with a metamorphic reheating overprint in the earliest Jurassic at ca. 200 Ma (Dallmeyer, 1984). Moreover, a diabase dike sample has a whole rock $^{40}Ar/^{39}Ar$ age of 190 Ma, which may indicate emplacement associated with the initial dismemberment of Pangea (Dallmeyer, 1984) due to rifting associated with the emplacement of the Central Atlantic Magmatic Province (Pindell et al., 2020).

Northern Maya Block – Chicxulub Impact Structure

Insights into the basement of the northern Maya Block are limited, with most data originating from the Chicxulub impact structure, where industry wells (Yucatán 1 and 4; Fig. 2) penetrated pre-Mesozoic igneous and metamorphic basement, including metavolcanic rocks and metaquartzite. Silurian Rb-Sr dates (410 Ma) were reported from rhyolite in the Yucatán 1 core, with a Carboniferous (300 Ma) metamorphic event (Lopez Ramos, 1975), and meta-andesite and dacite in that core recorded 290–330 Ma dates. Zircon U-Pb analyses produced a principal source age for Chicxulub target rocks of 550 Ma and minor 418 Ma and ca. 330 Ma target rock components (Kamo and Krogh, 1995; Kamo et al., 2011; Keppie et al., 2011; Krogh et al., 1993a, 1993b).

None of these age constraints derive from in-situ bedrock but rather from allochthonous breccia within the Chicxulub impact structure or worldwide K-Pg boundary deposits. Krogh et al. (1993a) performed thermal ionization mass spectrometry (TIMS) U-Pb analyses on 14 single zircon grains from distal ejecta deposits in the Raton Basin, Colorado, USA, K-Pg section. Krogh et al. (1993b) included two more sample locations (Haiti and Yucatán 6). Kamo and Krogh (1995) and Kamo et al. (2011) studied K-Pg sections in Saskatchewan, Spain, and Italy and presented new zircon U-Pb dates. All of these studies showed a discordia line with an upper concordia intercept of 544.5 ± 5 Ma that is anchored at 66.0 ± 0.5 Ma, which were interpreted as the basement and impact ages, respectively (Krogh et al., 1993a, 1993b; Kamo and Krogh, 1995; Kamo et al., 2011). A minor 418 Ma component links Haiti and Chicxulub as well (Kamo et al., 2011; Krogh et al., 1993a). In light of these results, most studies suggested that the northern Maya Block was predominantly composed of Pan-African (Brasiliano) crust with minor Early Devonian and Carboniferous magmatic additions (Krogh et al., 1993a, 1993b; Kamo and Krogh, 1995; Kamo et al., 2011; Keppie et al., 2011; Schmieder et al., 2017, 2018).

IODP/ICDP Expedition 364 drilled and sampled the peak ring of the Chicxulub impact structure with nearly 100% core recovery from ~506–1335 m below seafloor (mbsf) (Fig. 2B; Morgan et al., 2016; Morgan et al., 2017). The bottommost unit in the core (IV, ~750–1335 mbsf) consists of ~588 m of granitic basement that is crosscut by impact melt dikes, impact breccia dikes, and pre-impact dolerite, felsite, and granitoid dikes (Morgan et al., 2017). Impactites, including impact melt rock and suevite (impact melt-bearing breccia), were recovered in Units II and III from 617 mbsf to 748 mbsf, and Paleogene sediments were recovered in Unit I from 505 mbsf to 617 mbsf. Importantly for this study, Unit IV represents the uplifted granitic Maya Block basement. This core material represents the most substantial amount of basement from Chicxulub cores available, and Unit IV is not obviously similar to the small clasts of granitoid rocks observed in impact breccias in other boreholes (Gulick et al., 2017). Hence, this study provides critical new constraints on the age, tectonic affinity, and nature of this portion of the northern Maya Block.

Previous work dated the granitoids from the IODP Expedition 364 core (Schmieder et al., 2017; Xiao et al., 2017; Rasmussen et al., 2019; Timms et al., 2020; Zhao et al., 2020). However, these studies utilized smaller sample sizes than this study. A magmatic titanite in a lower peak ring granite sample from 887 mbsf gave a U-Pb concordia date of 341 ± 6 Ma (Schmieder et al., 2017). Timms et al. (2020) analyzed a shocked titanite from the IODP Expedition 364 impactites and produced a date of 307 ± 10 Ma. Rasmussen et al. (2019) observed two Carboniferous zircon crystals: a grain from 1310 mbsf with a date of 328 ± 2.4 Ma and a grain from 1330 mbsf with a date of 311 ± 5.4 Ma. Zhao et al. (2020) dated a subset of 40 zircons in five samples from the granitoids with a weighted mean age of 326 ± 5 Ma.

MATERIALS AND METHODS

In this study, we report detailed zircon U-Pb geochronological and trace-element geochemical data from 21 granitoid samples from the IODP-ICDP Expedition 364 Hole M0077A core (Fig. 2B). Samples were collected from the core by the science party at the IODP core repository in Bremen, Germany, in 2016 (Figs. 2B and 3). All samples selected are coarse-grained granitoids with varying percentages of pink alkali-feldspar, white to light yellowish plagioclase, interstitial gray to white quartz, and some biotite (Fig. 3). Samples were either 5 cm half rounds or 10 cm full rounds (see Appendix II[1]). Fracture zones, intrusions, and cataclasites were avoided. The sample numbers refer to the core and section number (i.e., sample 105R3 is from Core 105 Section R3); for specific sampled intervals, see Appendix II. Grain numbers are used when referring to one particular zircon analysis within a sample (i.e., 105R3#1). All analytical data are reported in Appendix II and are also available from geochron.org (accessed January 2021).

All LA-ICP-MS, mineral separation, and analytical work was carried out at the UTChron Geo-Thermochronometry Facility at The University of Texas at Austin. Zircon was separated from the core samples (Fig. 3) employing standard mineral separation techniques that included crushing and grinding, hydrodynamic, magnetic, and heavy liquid separation. Zircon crystals were hand-picked using a binocular microscope onto double-sided adhesive tape mounted on 1-

inch circular acrylic discs for depth profile LA-ICP-MS zircon U-Pb and REE analysis following the analytical procedures outlined in Marsh and Stockli (2015) and Rasmussen et al. (2019, 2020). LA-ICP-MS zircon depth profile analyses to a depth of 15–20 μm offer a way to more systematically resolve different zircon growth domains between rims and inherited cores of crystals as well as better quantification of Pb loss, and to impact-induced damage (Marsh and Stockli, 2015; Rasmussen et al., 2019, 2020).

Zircon U-Pb Depth-Profile Analysis

Unpolished zircon crystals were depth-profiled using a PhotonMachine Analyte G.2 193-nm Excimer Laser using a large-volume Helex cell attached to a Thermo Element2 ICP-MS with ablations carried out using a spot size of 25–30 μm for 30 seconds (s) at 10 Hz and a laser energy of 4 mJ. GJ1 zircon was used as the primary standard for both U-Pb and trace element analyses (601.7 ± 1.3 Ma; Jackson et al., 2004) and Plešovice (337.13 ± 0.37 Ma; Sláma et al., 2008) and 91500 zircon (1065 Ma; Wiedenbeck et al., 1995) as the secondary standards for U-Pb analyses to monitor procedural integrity and accuracy. LA-ICP-MS precision with 25–30 μm spot sizes is between 2% and 4% (Schoene, 2014). Primary and secondary standards were run as a block at the beginning and end of the analytical sequence as well as interspersed within the unknowns at a 5:1 (unknowns: standards) ratio.

U-Pb Data Reduction

We used Iolite (Hellstrom et al., 2008; Paton et al., 2011) and the VisualAge data reduction scheme (Petrus and Kamber, 2012) for data reduction of both the U-Pb and trace element data. The data were then exported with propagated errors and plotted on Wetherill Concordia diagrams using IsoplotR (Wetherill, 1956; Vermeesch, 2018). All reported uncertainties are 2σ. We did not perform a common Pb correction because the presence of Hg in the argon nebulizer gas interferes with ^{204}Pb. For zircon with ^{206}Pb/^{238}U ages younger than 850 Ma, concordant ^{206}Pb/^{238}U dates were used in weighted mean average calculations. Crystals were considered concordant if there was <15% discordance between the ^{206}Pb/^{238}U age and the ^{207}Pb/^{235}U age and if the ^{206}Pb/^{238}U age had <15% 2σ error. For ages older than 850 Ma, ^{207}Pb/^{206}Pb ages were reported and were considered concordant if there was <15% discordance between the ^{206}Pb/^{238}U age and the ^{207}Pb/^{206}Pb age.

As Rasmussen et al. (2019, 2020) described, most grains exhibit complex internal U-Pb systematics due to magmatic inheritance as well as Pb loss related to metamictization and/or impact-related hydrothermal alteration. In light of these complications, total average integration ages for single zircon do not offer the most meaningful way of deciphering the magmatic evolution of these basement rocks in the Chicxulub peak ring. To circumvent those difficulties caused by traditional bulk age reduction, where the entire laser ablation trace is used to calculate a single date, we examined the depth-profiled data second by second and only used a portion of the trace with the most stable plateau to calculate the "true age" of each grain. In this approach, we split a single 30 s ablation analysis into 1 s increments from a subset of the samples, which allowed us to carefully and systematically monitor age changes and U-Pb systematics through a single crystal (Marsh and Stockli, 2015; Rasmussen et al., 2019, 2020). Incremental ^{206}Pb/^{238}U ages for each 1 s increment were plotted against ablation time as age spectra (Rasmussen et al., 2019, 2020) to visualize the intra-grain U-Pb systematics. These Pb-loss, inheritance, and common Pb complexities are readily apparent when plotting the time-resolved, depth-profiling data for each zircon from this subset of samples.

After examining the subset of data in 1 s increments, it is apparent that the integration of the entire full-length ablation trace for a grain leads to systematic uncertainties that do not address the complexities in U-Pb systematics. Hence, to refine the crystallization ages recorded for all grains and the weighted mean age of each sample, we carefully selected “plateau ages” and applied discordance filters to minimize Pb loss and the inherited component. Also, in the workflow, we further filtered the age data by first statistically (>2σ) culling inherited and Pb-loss ages by obtaining weighted mean ^{206}Pb/^{238}U age calculations (Fig. 4 insets). Subsequently, we evaluated the ^{206}Pb/^{238}U data by progressively constricting discordance filters (15%, 5%, 3%, and 2%) to pinpoint the intrusion age.

REE Depth-Profile and Bulk Rock Analysis

In addition, we completed zircon LA-ICP-MS trace element analyses on a subset of the granitoid zircon crystals to understand their petrogenesis and tectono-magmatic affinity following the procedures outlined in Anfinson et al. (2016). Zircon grains were selected for trace element analyses if they were large enough to fit two 30 μm-diameter laser ablation spots (one spot for U-Pb, another spot for trace elements). NIST612 glass was included as a standard for trace element analyses (Kent, 2008). We measured ^{29}Si, ^{45}Sc, ^{49}Ti, ^{89}Y, ^{93}Nb, ^{139}La, ^{140}Ce, ^{141}Pr, ^{146}Nd, ^{147}Sm, ^{153}Eu, ^{157}Gd, ^{159}Tb, ^{163}Dy, ^{165}Ho, ^{166}Er, ^{169}Tm, ^{172}Yb, ^{175}Lu, ^{178}Hf, ^{181}Ta, ^{208}Pb, ^{232}Th, and ^{238}U. Trace element data were reduced using the “Trace_Elements” data reduction scheme in Iolite using ^{29}Si for the internal stoichiometric (15.3216 wt% Si) standardization and National Institute of Standards and Technology (NIST) 612 for the external concentration standard. All trace element analytical data are reported in Appendix II.

RESULTS

Overall, the entire granitic basement section is composed of relatively monotonous and variably shocked Carboniferous granite that yielded concordant U-Pb dates of euhedral to subhedral zircon crystals ranging from ca. 212 Ma to ca. 392 Ma (n = 658; Figs. 4–5) that are less than or equal to 15% discordant. The granitoid rocks are likely more voluminous at this location in the crater but were not cored in Hole M0077A. Systematic depth-profiling also revealed inherited zircon dates (n = 42) in 12 samples that provide insights into the basement ages of the northern Maya Block.

Zircon U-Pb Age Determination

Incremental Depth-Profile Zircon U-Pb Results

In an attempt to remove subjective user filtering and to better understand U-Pb systematics within single zircon crystals, we explored 1 s (~0.5-μm-deep) ablation increments as detailed by Rasmussen et al. (2019, 2020). This method allows for an improved determination of intra-grain U-Pb age topologies and definition of spatially coherent age domains ("U-Pb plateau ages"), which minimize the effects of Pb loss due to metamictization and mobilization due to hydrothermal alteration to derive robust granitic crystallization ages (Rasmussen et al., 2019). The incremental LA-ICP-MS U-Pb depth profiling technique (Marsh and Stockli, 2015; Rasmussen et al., 2019) allows for careful selection of U-Pb "plateau ages" in contrast to the conventional U-Pb dates, which integrate over the total ablation duration. If the total integration windows are used (conventional U-Pb dates), the ages tend to be systematically younger and there is evidence of more substantial Pb loss (Fig. 6, black labels). Three common patterns have been observed in our data set, including (1) Pb loss around the exterior rims of grains (Fig. 6A), (2) Pb loss/metamictization within the interior of the grains correlated with high [U] (Fig. 6B), and (3) stable total integration plateaus with portions of the grain having large uncertainties (Fig. 6C). Visual inspection of age variations within crystals allows for careful selection of coherent, undisturbed "plateau" age domains for these U-Pb plateau ages (Fig. 6, blue labels). We utilized incremental [U] data as a proxy for metamictization and damage in single grains to further refine U-Pb plateau ages by calculating a U-Pb age for the portion of the crystals with low [U] as was done for Figure 6B. These grains (Fig. 6) highlight the superiority of selecting U-Pb plateau ages and not using the total integration age when determining the ages of a single grain. Additionally, by improving single grain ages, we improve each sample's weighted mean ages and the age of the pluton.

We also qualitatively evaluated the possible effects of impact microstructure on grains by scanning electron microscopy based on the external morphology without polishing the grains (Fig. 7; Wittmann et al., 2006). Approximately 86% of the subset ($n = 250$) of crystals that we imaged had no external shock-related damage features or had minor fractures; 8% were severely fractured, and <6% displayed potential planar microstructures or possible granular textures. Conventional U-Pb ages (integrating over the total ablation signal) appear to decrease with increasing damage (Fig. 7). The degree of discordance and age spectra instability of the grains generally increases with younger ages and more damaged crystals (Fig. 7). Sample 105R3 grain #72 (Figs. 7A–7C) shows a Middle Cambrian zircon with an undisturbed 1 s age spectrum, where all increments are concordant and define a coherent plateau age and in which adjacent depth increments overlap within 2σ uncertainties. Sample 145R1 grain #22 (Figs. 7D–7F) shows a pristine Carboniferous crystal with a U-Pb plateau age of 348.8 ± 6.3 Ma and 7.7% discordance for the section of the grain that excludes Pb loss and high U concentration on the rim of the grain as well as inside the crystal. The incremental U-Pb ages in Figs. 7D–7F are younger in the center of the crystals, which Rasmussen et al. (2019) interpret as metamict zones within fractured zircon crystals, which indicates that intragrain U-Pb kinetics and/or hydrothermal fluid flow control age resetting in zircon rather than just impact-induced shock and heating. A highly fractured grain (105R3#1) had a U-Pb plateau date of 295.1 ± 2.81 Ma and 4.4% discordance, which was calculated using the flat latter part of the incremental U-Pb age spectra where the [U] is lower (~700 ppm) (Figs. 7G–7I). With careful investigation of the $^{206}Pb/^{238}U$, $^{207}Pb/^{235}U$, $^{207}Pb/^{206}Pb$, and [U], we selected coherent plateaus with low [U] to calculate single ages and robust mean sample ages.

Sample weighted mean U-Pb dates

Figure 5A shows sample mean ages for individual samples calculated for <15% and <5% discordance, respectively. Generally, the calculated ages are older when more rigorously filtered as most of the Pb-loss grains are removed. While the filtering reduces the intrasample scatter and improves the individual mean ages, the intersample variability persists and is larger than intrasample variability, as the sample mean ages (with 5% filter) exhibit significant overdispersion (high mean square of weighted deviates [MSWD]), which suggests that there is no systematic age trend with depth. Even with the tightest discordance filters, concordant ages in the different samples will display a large range of ages. Therefore, we chose to combine all of the Carboniferous (non-inherited) zircon grains to calculate a single weighted mean age for all samples (Fig. 5B). Figure 5B shows a Kernel Density Estimation (KDE) of all Carboniferous grains with sample weighted mean calculated for each filter. The 15% discordance filter gives a combined age of 324.7 ± 1.3 Ma (95% confidence interval) for 538 grains (MSWD = 140), while the 5% filter yielded a combined age of 331.9 ± 2.4 Ma for 342 grains (MSWD = 43.1). An age of 333.9 ± 2.1 Ma is obtained from 235 grains passing through the 3% discordance filter (MSWD = 38.3). The 2% discordance filter yields an age of 334.3 ± 2.3 Ma for 166 grains (MSWD = 33.1). The results for the combined ages using 5%, 3%, and 2% discordance filters all overlap within their 95% confidence intervals and are within less than 2 Ma for their weighted mean age. As the filters tighten, the means converge at ca. 334 Ma, which suggests that this result is the most robust estimate for the crystallization age of the pluton. The MSWD calculations (43.1, 38.3, and 33.1, respectively) are high, and this is likely attributable to both the small individual errors and scatter along concordia over a relatively wide range between 380 Ma and 300 Ma even for grains with <2% discordance. We hypothesize that this scatter and subtle Pb loss is likely attributable to both late Carboniferous and Permian hydrothermal and magmatic activity as well as K-Pg, impact-related Pb loss that is not resolvable in terms of discordance given the analytical precision.

Table 1 describes sample weighted mean ages calculated from data filtered at <15% and <5% discordance with uncertainties reported as the 95% confidence interval as well as how many grains passed through each filter. With the 15% discordance filter, the samples' weighted mean ages range from ca. 310 Ma to ca. 338 Ma, and after implementing the 5% discordance filter the weighted mean ages range from ca. 311 Ma to ca. 344 Ma (Fig. 5A; Table 1). See Appendix II for raw zircon U-Pb results (see [footnote 1]).

Eleven grains from samples 105R3 (n = 5),145R1 (n = 4), 209R2 (n = 1), and 235R2 (n = 1) exhibited rim-core age relationships where both the rim and the core were <30% discordant. Four grains preserved core dates between 355 Ma and 377 Ma and rim dates between 315 Ma and 331 Ma (see Appendix I).

Inherited Zircon Component

Beyond age constraints for the intrusive granitic rocks in the Chicxulub peak ring, the depth profile U-Pb analysis also provides insights into the basement history of the northern Maya Block from xenocrystic zircon grains and inherited zircon cores. Inherited pre-Carboniferous zircon ages (n = 42) from all samples are characterized by Silurian-Devonian (ca. 440–400 Ma, n

= 11), Ediacaran-Cambrian (ca. 630–500 Ma, n = 11), and Mesoproterozoic (ca. 1300–1000 Ma, n = 20) age groups (Fig. 8). Sample 235R3 (~1123 msbf) had Peri-Gondwanan (n = 2) grains, which had a rim with an age of 322 ± 13 Ma. Sample 302R1 (~1330 msbf) revealed the oldest zircon grain with an age of 1976 ± 20 Ma. There is no systematic trend with core depth of inherited zircon components or magmatic age, so these samples are all from the same pluton.

Zircon REE Geochemistry

Magmatic zircon crystals not only preserve U-Pb crystallization ages but also trace element compositions and, therefore, have the potential to shed light on the tectonic setting of magmatism. We selected a subset of zircon grains (n = 235) from five samples from the granitoid basement recovered in the Expedition 364 Hole M0077A for trace element analysis guided by the zircon U-Pb age determinations.

The chondrite-normalized REE concentrations of Carboniferous zircon grains show positive Ce anomalies and slightly positive Eu anomalies (McDonough and Sun, 1995; Fig. 9). There is a spread in concentrations of light REE (LREE), which correlates with younger ages (Fig. 9). The average Th/U is 0.48 but varies from 0.13 to 7.37. The average Ce/Ce* anomaly is 7.53 and the average Eu/Eu* anomaly is 0.73 based on the calculations in Trail et al. (2012). Zircon trace element ratios are plotted in discrimination plots (Fig. 10; Grimes et al., 2015). The majority of the zircon grains plot within the continental arc field of the discrimination diagram based on their characteristic heavy REE (HREE)-LREE ratios.

DISCUSSION

Depth profile zircon U-Pb geochronology and trace element geochemistry presented here provide a large new data set of crystallization ages and REE concentrations for the northern Maya Block preserved within the NW peak ring of the Chicxulub impact structure. Building on previously reported regional ages, our zircon data set chronicles Carboniferous arc magmatism along the northern margin of the Maya Block at 334.0 ± 2.3 Ma. This age is coincident with the closing of the Rheic Ocean as Gondwana approached Laurentia and implies southward subduction of oceanic lithosphere beneath the Maya Block (Fig. 11). Furthermore, three distinct inherited age groups shed light on the crustal evolution of the Maya Block and include Peri-Gondwanan, Pan-African, and the Grenvillian tectono-magmatic episodes (Figs. 4 and 8). The inherited Grenvillian and Pan-African zircon ages that contaminate the Carboniferous granitoids require a more evolved crustal source; thus, they are consistent with a continental magmatic arc origin for the peak ring granites.

Continental Arc Magmatism produced by Rheic Ocean Subduction

In addition to a brief, shock-related heating pulse that induced a temperature increase on the order of 170 °C (Kring et al., 2020), the Maya Block basement granites at Hole M0077A are locally hydrothermally altered by the emplacement of pre-impact dikes and low-grade metamorphism that is expected for their pre-impact depths of 8–10 km and an average continental geothermal gradient (Morgan et al., 2016; Gulick et al., 2017; Wittmann et al., 2018; Kring et al., 2020). Additional alteration is expected by post-impact hydrothermal activity (Kring et al., 2020). Based on adakitic whole rock geochemistry of the granites, Zhao et al. (2020) suggested a crustal anatexis origin for the Hole M0077A granite caused by asthenospheric upwelling resulting from slab breakoff. One or a combination of these different hydrothermal alteration events could potentially affect the whole-rock geochemical signature of the granitoids, specifically fluid mobile elements such as K, Na, La, and Sr (as is shown in de Graaff et al., 2021). Generally, the granite bulk rock data indicate depletion of HREE and enrichment in LREE compared to chondritic values (de Graaff et al., 2021). They exhibit depleted Nb and Ta signatures but moderate Zr and Hf enrichment, which is typical of arc-type magmatism (Pearce et al., 1984). Yb and Ta concentrations from bulk rock analyses plot in the volcanic arc granite field of the discrimination diagram from Pearce et al. (1984) and de Graaff et al. (2021).

In contrast, geochemical signatures of concordant zircon grains are less altered by open system behavior after initial crystallization and, therefore, reflect the original REE patterns of the magmatic system (Rubatto, 2002). The interpretation of slab breakoff-related granite origin from Zhao et al. (2020) is inconsistent with our new age (334.0 ± 2.3 Ma), which is 8 m.y. older than the age presented in Zhao et al. (2020). However, even with the tightest discordance filtering, there is a persistent subset of grains that cluster ca. 317 Ma (Fig. 5B). We believe that the ca. 326 Ma age (Zhao et al., 2020) is younger than our preferred age (ca. 334) because it averages the two clusters of ages (334 Ma and 317 Ma). We propose that this Pennsylvanian zircon age cluster is the result of Pb loss in response to spatially heterogeneous reheating or hydrothermal fluid flow during slab breakoff or incipient continent collision. The notion of spatially heterogenous age reduction appears to be supported by the fact that younger ages are restricted to only four samples (Fig. 5A, Table 1; 106R2, 107R3, 157R1, and 209R2) and do not correlate with U concentration or metamictization level. We hypothesize that this localized 317 Ma Pb loss is linked to the emplacement of cross-cutting felsite dikes characterized by the high K_2O content, LREE enrichment, and positive εNd, which is suggestive of a metasomatic mantle from slab fluids due to slab breakoff (Zhao et al., 2020). This igneous activity is similar in age to that to the southeast in the Altos Cuchumatanes, where the magmatism occurred between 317 Ma and 312 Ma (Solari et al., 2010).

A slab breakoff at ca. 334 Ma is implausible as subduction persisted through the latest Mississippian (Nance and Linnemann, 2008), which supports the fact that the granitoid rocks in the Maya Block formed due to subduction zone arc magmatism and predate closure of the Rheic Ocean and initial continental collision. Deformation in the Ouachita-Marathon foreland fold and thrust belt developed in the middle Pennsylvanian (ca. 308 Ma; Viele and Thomas, 1989; Thomas et al., 2019) and at least ca. 10–20 m.y. after the arc magmatism dated in this study.

The REE signatures of the Carboniferous zircon grains plot in the continental magmatic arc field (Fig. 10) and do not exhibit asthenospheric signatures as one would expect if related to slab breakoff. The chondrite-normalized REE pattern is characterized by flatter LREE and steep HREE slopes as well as positive Ce anomalies and slightly positive Eu anomalies that are typical for magmatic arc systems (Rubatto, 2002; Hoskin and Schaltegger, 2003; Burnham et al., 2015). The positive Ce/Ce* values have been interpreted to correlate with an increased oxidation state of the melt (Trail et al., 2012), whereas the lack of an Eu anomaly may point to oxidizing fluids (Rubatto, 2002; Hoskin and Schaltegger, 2003; Burnham et al., 2015). Using the classification in Hoskin (2005), our zircon analyses mainly plot in between the magmatic and hydrothermally altered fields and are characterized by moderate La concentrations, flatter LREE slope $(Sm/La)_N$, and moderate Ce anomalies (see Appendix I). However, most geochemical evidence points to a magmatic nature and the limitations of this classification scheme. The bulk rock geochemistry shows that La, which is usually an immobile element, was mobilized during the Chicxulub impact (de Graaff et al., 2021). This may account for some of the spread in the zircon REE discrimination plots.

The Carboniferous zircon age and REE patterns record Mississippian continental arc magmatism as a result of the closing of the Rheic Ocean prior to the continental collision of Gondwana and Laurentia along the Ouachita-Marathon suture in the late Carboniferous-Early Permian (Thomas, 2010). Evidence of subduction has also been identified in the Acatlán Complex within the southern Oaxacan terrane in light of Carboniferous-aged eclogites, high-pressure schists, and migmatites (Estrada-Carmona et al., 2016; Middleton et al., 2007; Vega-Granillo et al., 2007). Keppie et al. (2008) suggested that the muted detection of the arc may be due to subduction erosion beneath the Oaxacan/Gondwanan margin. However, our results show that although the Maya Block has Gondwanan affinity based on the inherited Pan-African ages, the arc is preserved and not eroded within the northern Maya Block. Additionally, middle Mississippian to Early Permian detrital zircon and volcanic detritus in southern Laurentia document the approaching arc in the Ouachita and Marathon areas as sediments are shed from sediments on the Gondwanan side of the suture and onto the Laurentian side of the suture and into the Marathon and Permian Basins (Gleason et al., 2007; Shaulis et al., 2012, Soreghan and Soreghan, 2013; Liu and Stockli, 2020; Soto-Kerans et al., 2020, and references therein). These reconstructions are consistent with Peri-Gondwanan terranes having been located along the Gondwanan margin until the final assembly of Pangea. In the Mesozoic, while portions of these terranes remained affixed to the Laurentian margin during rifting and Pangea breakup, other Peri-Gondwanan terranes fragmented or rifted away from Laurentia. Rotation and translation of the Maya Block away from Laurentia occurred during the Middle Jurassic opening of the Gulf of Mexico (Pindell and Dewey, 1982; Dickinson and Lawton, 2001; Mann et al., 2007) until seafloor spreading ceased and spreading shifted to the south of the Maya Block into the proto-

Caribbean realms, which left the Maya Block and the rest of the Mexican terranes as part of North America.

Evidence for Regional Carboniferous Continental Arc Magmatism

The similarities in the tectono-magmatic evolution of the Coahuila and Suwannee terranes with the northern Maya Block suggest that these regions likely represent a contiguous Carboniferous convergent margin along the northwestern corner of Gondwana. In the Coahuila terrane of northern México (Figs. 1 and 11), the Las Delicias contains a record of late Paleozoic arc magmatism as indicated by the Pesuña peperite pluton (331 ± 4 Ma) and a dacitic ignimbrite (303 ± 13 Ma) (Lopez, 1997; Lopez et al., 2001; McKee et al., 1999). In addition, early Mesozoic strata in basins adjacent to the Coahuila terrane (Sierra El Granizo, Valle San Marcos, and La Gavia anticline) contain detrital zircon U-Pb spectra characterized by a peak between ca. 370 Ma and 280 Ma as well as age peaks at 1040 Ma, 562 Ma, 422 Ma, and 414 Ma (Thomas et al., 2019). In the Huizachal-Pergrina anticlinorium, the Mesoproterozoic Novillo Gneiss Complex is overlain by the Carboniferous Aserradero Rhyolite (ca. 334 Ma) with inherited zircon cores of ca. 1086 Ma (Stewart et al., 1999) that are similar to those in this study (Figs. 1 and 11). Most recently, the Asserradero Rhyolite yielded two ages from different samples: 347.8 ± 2.7 Ma and 340.7 ± 3.6 Ma with inherited grains ranging from 1.0–1.4 Ga (Ramírez-Fernández et al., 2021). The Granjeno Schist in the same area has an intrusion age of 351 ± 54 Ma (U-Pb in zircon) and a cooling age of 313 ± 7 Ma ($^{40}Ar/^{39}Ar$ in muscovite; Dowe et al., 2005). These magmatic rocks and metamorphic cooling ages likely formed the NW corner of the continental subduction zone to accommodate the final assembly of Pangea and were subsequently offset from the northern Maya Block by the East Mexican transform during the Jurassic opening of the Gulf of Mexico.

Within the Suwannee terrane, there is evidence for Carboniferous arc magmatism from basement well penetrations in Georgia, Alabama, and Florida (Figs. 1 and 11; Heatherington and Mueller, 1997; Mueller et al., 2014). This includes the Elberton batholith, Bald Rock, Edgefield, Siloam, Winnsboro, and Liberty Hill granite with ages ranging from ca. 304–326 Ma (Dallmeyer et al., 1986; Dennis and Wright, 1997; Heatherington and Mueller, 1997; Samson, 2001). However, given the diachronous closure of the Rheic Ocean and the oblique collision between Laurentia and Gondwana, some studies suggested that these granitic rocks could already be post-orogenic in nature and related to lithospheric delamination (Heatherington et al.; 2010; Mueller et al., 2014).

Deep Sea Drilling Project (DSDP) Leg 77 at Site 537 and Hole 538A recovered pre-Mesozoic gneissic basement between the Yucatán and Florida near the present-day Campeche Escarpment (Figs. 1 and 11; Dallmeyer, 1984), which yielded a biotite $^{40}Ar/^{39}Ar$ plateau age of 348 ± 8 Ma that was suggested to be due to open system behavior during a ca. 190 Ma thermal event (Dallmeyer, 1984). Our new U-Pb data from the basement at IODP Expedition 364 Site M0077, Hole M0077A, however, suggest that these $^{40}Ar/^{39}Ar$ dates could be associated with Carboniferous arc magmatism (Fig. 11). The ca. 190 Ma diabase emplacement was likely linked to the initial extension and dismemberment of Pangea (Dallmeyer, 1984) and may be similar to the diabase dikes encountered in Hole M0077A.

In southern Oaxaquia, the paragneisses, granites, and charnockites are intruded by or overlain by Carboniferous granitoids and felsic lavas, respectively (Ortega-Obregón et al., 2014), such as the Cuañana pluton, which yielded a zircon U-Pb date of 311 ± 2 Ma. The spatial and temporal transition from Late Carboniferous Rheic to Late Permian Pacific subduction and arc magmatism remains unclear (Coombs et al., 2020; Ortega-Obregón et al., 2014). However, the

Carboniferous arc magmatic rocks of the Coahuila, Suwannee, and northern and southern Maya Block correlate in space and time and likely formed a coherent group of Peri-Gondwanan terranes that were intruded by continental arc magmatism related to the closure of the Rheic Ocean (Fig. 11).

Early Paleozoic and Proterozoic Tectono-Magmatic Evolution

A small subset of zircon analyses from the Hole M0077A core yielded U-Pb ages between 500 Ma and 400 Ma (Fig. 8) that are similar to ages found in the Maya Mountains and as a minor component in Chicxulub breccias and worldwide K-Pg boundary sections (Krogh et al., 1993a; Kamo and Krogh, 1995; Steiner and Walker, 1996). These Peri-Gondwanan ages, which are related to deformation and magmatism along the transform margin between Laurentia and Gondwana, support a paleo-position of the Maya Block along the northwestern margin of Gondwana alongside other Peri-Gondwanan terranes including Oaxaquia and Suwanee (Keppie et al., 2011).

In addition to these Ordovician-Devonian ages, we also observed inherited Pan-African zircon ages (Fig. 8) that we interpreted as evidence for Neoproterozoic magmatic or metasedimentary Peri-Gondwanan basement that was later intruded by a younger volcanic arc. Ages between 465 Ma and 550 Ma are found in Yucatán 6 core breccia clasts (n = 6; Kettrup and Deutsch, 2003) and Yaxcopoil 1 (n = 33; Keppie et al., 2011) as well as K-Pg boundary sections in Colorado, Saskatchewan (Krogh et al., 1993a, 1993b; Kamo and Krogh, 1995), Spain, and Italy (Kamo et al., 2011; Fig. 8). See Appendix I for chronometers used and more details. To the NE of Yucatán, in samples from DSDP Leg 77, hornblende $^{40}Ar/^{39}Ar$ age spectra recorded cooling ages of ca. 500 Ma (Dallmeyer, 1984), which is indicative of a pervasive Peri-Gondwanan orogenic imprint on the northernmost Maya Block.

The oldest group of inherited U-Pb ages observed in this study is linked to the Mesoproterozoic Grenvillian Oaxaquia terrane (0.9–1.4 Ga; Fig. 8). These ages suggest that the Maya Block was linked to the Oaxaquian belt (Weber et al., 2018). This is also supported by Chicxulub granitic gneiss clasts from the Yucatán 6 borehole that yielded T_{DM} model ages of 1.2–1.4 Ga (Kettrup et al., 2000) and impact melt rocks that gave model ages of ca. 1.06 Ga (Blum et al., 1993) and 1.1–1.2 Ga (Kettrup et al., 2000). Zhao et al. (2020) obtained slightly younger Nd model ages (T_{DM2}) of 1.03–1.07 Ga from the Hole M0077A granite samples. All of these observations are consistent with the observed Mesoproterozoic inherited zircon, which points to a Grenvillian crustal component in the northern Maya Block. Overall, inherited zircon ages recovered from the Carboniferous basement in this study likely stem from Silurian-Early Devonian, Ediacaran, and Mesoproterozoic igneous rocks assimilated during Carboniferous arc magmatism and corroborate previously reported U-Pb zircon and T_{DM} ages recording Grenvillian, Pan-African, and Famatinian tectonic events typical of Peri-Gondwanan terranes (Figs. 8 and 11).

Furthermore, these new data support a link between southern and northern portions of the Maya Block on the basis of the following observations: (1) 1.4–0.9 Ga zircon cores within the El Triunfo Complex (González-Guzmán et al., 2016) similar to the inherited zircons; (2) Ediacaran and early Paleozoic sedimentary rocks in Belize with common Mesoproterozoic detrital zircon (e.g., Weber et al., 2012); (3) Ordovician-Silurian zircon in the southern Chiapas Massif Complex that is only slightly older than the inherited zircon (Estrada-Carmona et al., 2012); (4) Mississippian detrital zircon in the Carboniferous Santa Rosa Formation east of the Chiapas Massif (e.g., Weber et al., 2009); and (5) abundant Ediacaran detrital zircons in the Santa Rosa Formation similar to the inherited zircon component (e.g., Weber et al., 2009). The inherited zircon in the Chicxulub Carboniferous basement is also similar to detrital zircon from the Jocote unit in the El Triunfo Complex and the Badly unit in Belize with ages of 1.5 Ga, 1.2 Ga, and 1.0–0.9 Ga, which suggests a similar metasedimentary basement component for both Belize and the El Triunfo Complex (Estrada-Carmona et al., 2012; Weber et al., 2012). Overall, detrital zircon and metamorphic ages of the southern Maya Block are similar to those of the northern Maya Block (this study) and do not support a separate Paleozoic history or separate sub-terranes with different tectono-magmatic evolutions as was suggested by Ortega-Gutiérrez et al. (2018).

Regional Similarities in Early Paleozoic and Proterozoic Evolution

In the Coahuila terrane, granitic and gneissic clasts within the Las Uvas conglomerate of the Late Permian Las Delicias Formation yielded U-Pb zircon ages of 1232 ± 7 Ma, 1214 ± 2 Ma, and 580 ± 4 Ma as well as a $T_{DM\ (Nd)}$ model age of 1394 Ma, which points to the derivation of the clasts from Pan-African and Oaxaquian basement (Lopez et al., 2001). Geochemically, the Grenvillian zircon results plot within the volcanic arc field (similar to Fig. 10), while the Pan-African grains plot within the "intra-plate granite" field (Lopez et al., 2001).

Our new constraints on inherited zircon components from the Carboniferous arc also support a genetic link between the Tamaulipas Arch and the Maya Block. Early Ediacaran enriched mid-oceanic-ridge basalt (E-MORB) amphibolite dikes in the El Triunfo Complex (southern Maya Block) dated at ca. 615 Ma are related to final Rodinia breakup and Iapetus opening (Weber et al., 2020) and are similar to E-MORB dikes from Novillo (ca. 619 Ma; Weber et al., 2019). However, no Ediacaran (ca. 550 Ma) granitic rocks have been reported from the southern Maya Block. Oaxaquia basement is composed of the Novillo Gneiss (1235–1115 Ma), which is intruded by anorthosite and related intrusive rocks at 1035–1010 Ma and metamorphosed under granulite facies conditions at 990 ± 5 Ma (Trainor et al., 2011).

The Suwannee terrane also hosts evidence for Pan-African orogenic events in the form of 600–700 Ma and 552 Ma granitic plutons in southern Alabama and Florida, USA (Heatherington et al., 1996). $^{40}Ar/^{39}Ar$ ages in northeastern Florida range from 535 Ma to 527 Ma in the Osceola granite (Dallmeyer et al., 1986) and 513–511 Ma in the St. Lucie Metamorphic Complex (Dallmeyer, 1989b). These Neoproterozoic to Early Cambrian ages are consistent with studies that placed the Suwannee terrane at the edge of western Gondwana alongside other peri-Gondwanan terranes. Heatherington et al. (2010) analyzed granitic well samples from the Suwannee terrane and obtained Carboniferous zircon U-Pb ages with xenocrystic ages of 1.0–1.2 Ga, which are very similar to those of the Maya Block basement presented in this study.

The data from the Coahuila Block and Novillo basement in NE México show similarities to our new data from the northern Maya Block and, along with the similarities in Carboniferous magmatism, strongly support the notion that the two blocks shared a common pre-Mesozoic history and formed a coherent terrane along the Gondwana margin prior to being dismembered and offset along the East Mexican transform during the Mesozoic Gulf of Mexico opening. The Suwannee terrane also shows a similar pre-Mesozoic, tectono-magmatic evolution, which suggests that it represents a portion of the same Peri-Gondwanan margin before subduction and closure of the Rheic Ocean (Fig. 11).

Implications for K-Pg ejecta studies

Our new zircon U-Pb data also have implications for Chicxulub ejecta deposits that warrant a new look at existing data. Concordant Late Devonian to Early Permian zircon U-Pb ages have been observed in ejecta layers and breccia clasts from the Chicxulub impact structure. Early Paleozoic ages are reported in the Chicxulub breccia from the Yucatán 6 core (Krogh et al., 1993b), Yaxcopoil 1 impact melt (Schmieder et al., 2018), Haiti, Raton Basin in Colorado

(Krogh et al., 1993b; Premo and Izett, 1993), Saskatchewan (Kamo and Krogh, 1995), and Spain (Kamo et al., 2011). Previous zircon ejecta studies suggest a minor component of target rock sequence that is younger than the dominant Pan-African signature. The re-evaluation of these data shows that the minor Carboniferous component is likely linked to a particular portion of impact target rocks and is now linked to a tectonic process that is not related to impact-induced Pb loss. The utility of zircon studies in describing impact target rock sequences provides more data to link target rocks to ejecta in distal locations.

CONCLUSIONS

Our geochronological and geochemical zircon analyses suggest the presence of a Carboniferous continental magmatic arc along the northern margin of the Maya Block. The location of this magmatic arc suggests a southward subduction polarity of the Rheic oceanic plate beneath Gondwana and Peri-Gondwanan terranes during the closure of the Rheic Ocean. Our ages also show that arc magmatism predates final Pangea amalgamation and is not related to Ouachita-Marathon continental collision or slab breakoff. We present data for 846 zircon grains that were depth-profiled to investigate the U-Pb systematics and to robustly define the granitic crystallization ages and the basement inheritance to shed light on the pre-Mesozoic evolution of the northern Maya Block. The analyzed zircon grains yielded concordant Carboniferous U-Pb ages with a weighted mean age of 334 ± 2.3 Ma using 166 grains that are <2% discordant. Ce and Eu anomalies, Th/U, and HREE-LREE data confirm a continental magmatic arc setting for the analyzed pluton.

Inherited zircon U-Pb ages (>400 Ma) in the granitoid basement are dominated by Early Devonian-Silurian, Cambrian-Ediacaran, and Mesoproterozoic modes. The age modes show that the Carboniferous granitic plutons intruded into older Gondwanan continental basement of the northern Maya Block with a tectono-magmatic history that resembles that of the Coahuila, Oaxaquia, and Suwannee terranes. These similarities suggest that these terranes formed a coherent Peri-Gondwanan margin prior to the late Paleozoic assembly and Mesozoic breakup of western Pangea.

Importantly, these new data also show that minor components of Carboniferous, as well as Peri-Gondwanan/Pan-African zircon from proximal and distal K-Pg ejecta layer sites, were likely derived from the Chicxulub target rock in the Maya Block. These data also indicate that Carboniferous zircon grains in K-Pg boundary layer sites, along with Pan-African grains, can be used as ejected tracers of the target rock.

ACKNOWLEDGMENTS

This research used samples and data provided by the International Ocean Discovery Program. Samples can be requested from http://web.iodp.tamu.edu/sdrm (accessed February 2021). Expedition 364 was jointly funded by the European Consortium for Ocean Research Drilling (ECORD) and the International Continental Scientific Drilling Program with contributions and logistical support from the Yucatán State Government and Universidad Nacional Autónoma de México (UNAM). This research was supported by the U.S. Science Support Program and National Science Foundation grant OCE-1737351, and D.A. Kring and M. Schmieder were supported by NSF-OCE 1766826. The work of P. Claeys and S.J. de Graaff on Chicxulub is supported by Research Foundation Flanders (FWO), Belgian Science Policy Office (BELSPO), and the VUB Strategic Research program. A. Wittmann is supported by NSF-OCE 1737087. D.F. Stockli acknowledges support from the University of Texas Chevron (Gulf) Centennial Professorship. J.V. Morgan was supported by NERC NE/P005217/1. Luigi Solari and Bodo Weber provided very helpful comments that led to improvements in the clarity and content in this manuscript. We also thank James Manor for assistance with scanning electron microscope imaging, Carole Lakrout and Claire Clifton for assistance with mineral separation, Lisa Stockli for assistance with U-Pb analyses, and the Stockli Group for their help and support while conducting the analyses at UT Austin. This is UTIG Contribution no. 3774, LPI Contribution no. 2593, and Center for Planetary Systems Habitability Contribution no. 0027. This is LPI Contribution 2593.

REFERENCES CITED

Alemán-Gallardo, E.A., Ramírez-Fernández, J.A., Rodríguez-Díaz, A.A., Velasco-Tapia, F., Jenchen, U., Cruz-Gámez, E.M., León-Barragán, L.D., León, I.N.-D., 2019. Evidence for an Ordovician continental arc in the pre-Mesozoic basement of the Huizachal–Peregrina Anticlinorium, Sierra Madre Oriental, Mexico: Peregrina Tonalite. Mineral Petrology, v. 113, p. 505–525. https://doi.org/10.1007/s00710-019-00660-4

Alvarez, W., 1996. Trajectories of ballistic ejecta from the Chicxulub crater *in* Ryder, G., Fastovsky, D., Gartner, S., eds., The Cretaceous-Tertiary Event and Other Catastrophes in Earth History: Geological Society of America Special Paper 307, p. 141 – 150.

Alvarez, L.W., Alvarez, W., Asaro, F., Michel, H.V., 1980. Extraterrestrial Cause for the Cretaceous-Tertiary Extinction. Science, v. 208, p. 1095–1108. doi:10.1126/science.208.4448.1095

Anfinson, O.A., Malusà, M.G., Ottria, G., Dafov, L.N., Stockli, D.F., 2016. Tracking coarse-grained gravity flows by LASS-ICP-MS depth-profiling of detrital zircon (Aveto Formation, Adriatic foredeep, Italy). Marine Petroleum Geology, v. 77, p. 1163–1176. https://doi.org/10.1016/j.marpetgeo.2016.07.014

Artemieva, N., Morgan, J., 2009. Modeling the formation of the K–Pg boundary layer. Icarus, v.

201, p. 768–780. doi:10.1016/j.icarus.2009.01.021

Artemieva, N. and Morgan, J., 2020. Global K-Pg layer deposited from a dust cloud. Geophysical Research Letters, 47, p.e2019GL086562.

Bateson, J.H. and Hall, I.H.S., 1977. The geology of the Maya Mountains: Belize: Institute of Geological Science. Her Majesty's Stationery Office, Overseas Memoir, v. 3, p.43.

Blum, J.D., Chamberlain, C.P., Hingston, M.P., Koeberl, C., Marin, L.E., Schuraytz, B.C., Sharpton, V.L., 1993. Isotopic comparison of K/T boundary impact glass with melt rock from the Chicxulub and Manson impact structures. Nature, v. 364, p. 325.

Bullard, E., Everett, J.E., Smith, A.G., 1965. The fit of the continents around the Atlantic. Philosophical Transactions of the Royal Society, ser. A, v. 258, p. 41–51.

Burnham, A.D., Berry, A.J., Halse, H.R., Schofield, P.F., Cibin, G., Mosselmans, J., 2015. The oxidation state of europium in silicate melts as a function of oxygen fugacity, composition and temperature. Chemical Geology, v. 411, p. 248–259.

Cameron, K.L., Lopez, R., Ortega-Gutiérrez, F., Solari, L.A., Keppie, J.D. and Schulze, C., 2004. U-Pb geochronology and Pb isotopic compositions of leached feldspars: Constraints on the origin and evolution of Grenville rocks from eastern and southern Mexico. Geological Society of America Memoirs, v. 197, p.755-769.

Cisneros de León, A.C., Weber, B., Ortega-Gutiérrez, F., González-Guzmán, R., Maldonado, R., Solari, L., Schaaf, P., Manjarrez-Juárez, R., 2017. Grenvillian massif-type anorthosite suite in Chiapas, Mexico: Magmatic to polymetamorphic evolution of anorthosites and their Ti-Fe ores. Precambrian Research, v. 295, p. 203–226.

Claeys, P., Kiessling, W. and Alvarez W., 2002. Distribution of Chicxulub ejecta at the Cretaceous-Tertiary Boundary *in* Koeberl C. MacLeod K.G., eds., Catastrophic Events and Mass Extinction: Impacts and Beyond: Geological Society of America Special Paper 356, p. 55–69.

Collins, G., 2002. Hydrocode Simulations of Chicxulub Crater Collapse and Peak-Ring Formation. Icarus, v. 157, p. 24–33. doi:10.1006/icar.2002.6822

Collins, G.S., Morgan, J., Barton, P., Christeson, G.L., Gulick, S., Urrutia, J., Warner, M., Wünnemann, K., 2008. Dynamic modeling suggests terrace zone asymmetry in the Chicxulub crater is caused by target heterogeneity. Earth and Planetary Science Letters, v. 270, p. 221–230. doi:10.1016/j.epsl.2008.03.032

Collins, G. S., Patel, N., Davison, T. M., Rae, A. S. P., Morgan, J. V., Gulick, S. P. S., and IODP-ICDP Expedition 364 Science Party, 2020. A steeply-inclined trajectory for the Chicxulub impact: Nature Communications, v. 11 no. 1, p. 1-10. https://doi.org/10.1038/s41467-020-15269-x

Compston, W., Williams, I. S., Jenkins, R. J. F., Gostin, V. A., and Haines, P. W., 1987. Zircon age evidence for the Late Precambrian Acraman ejecta blanket. Australian Journal of Earth Sciences, v. 34 no. 4, p. 435-445.

Coombs, H., Kerr, A., Pindell, J., Buchs, D., Weber, B. and Solari, L., 2019. Petrogenesis of the crystalline basement along the western Gulf of Mexico: Postcollisional magmatism during the formation of Pangea *in* Martens, U., Molina Garza, R.S., eds., Southern and central Mexico: basement framework, tectonic evolution, and provenance of Mesozoic-Cenozoic basins. Geological Society of America, Special Paper 546.

Dallmeyer, R.D., 1984, $^{40}Ar/^{39}Ar$ ages from a pre-Mesozoic crystalline basement penetrated at Holes 537 and 538a of the Deep Sea Drilling Project Leg 77, southeastern Gulf of Mexico: Tectonic implications: College Station, Texas, Deep Sea Drilling Program, Initial Reports, v. 77, p. 497–504

Dallmeyer, R.D., Wright, J.E., Secor JR, D.T., Snoke, A.W., 1986. Character of the Alleghanian orogeny in the southern Appalachians: Part II. Geochronological constraints on the tectonothermal evolution of the eastern Piedmont in South Carolina. Geological Society of America Bulletin, v. 97, p. 1329–1344.

Dallmeyer, R.D., 1988. Tectonic implications of $^{40}Ar/^{39}Ar$ ages from a pre-Mesozoic metamorphic basement penetrated on Leg 77 of the Deep Sea Drilling Project in the southern Gulf of Mexico. Journal of African Earth Sciences (and the Middle East), v. 7, no. 2, p. 443-449.

Dallmeyer, R.D., 1989a. Contrasting accreted terranes in the southern Appalachian Orogen, basement beneath the Atlantic and Gulf Coastal Plains, and West African orogens. Precambrian Research, v. 42, p. 387–409. https://doi.org/10.1016/0301-9268(89)90021-1

Dallmeyer, R.D., 1989b. A Tectonic Linkage between the Rodelide Orogen (Sierra Leone) and the St. Lucie Metamorphic Complex in the Florida Subsurface. Journal of Geology, v. 97, p. 183–195. https://doi.org/10.1086/629293

Dalziel, I.W., 1997. OVERVIEW: Neoproterozoic-Paleozoic geography and tectonics: Review, hypothesis, environmental speculation. Geological Society of America Bulletin, v. 109, p. 16–42.

Dawe, S.E., 1984. The geology of the Mountain Pine Ridge area and the relation of the Mountain Pine Ridge granite to the Late Paleozoic and early Mesozoic geological history, Belize, Central America. [Ph.D. thesis]: State University of New York at Binghamton.

de Graaff, S.J., Kaskes, P., Déhais, T., Goderis, S., Debaille, V., Feignon, J.-G., Ferrière, L., Koeberl, C., Ross, C.H., and Claeys, Ph., 2019, Making (More) Sense of Destruction – A

Comprehensive Geochemical Investigation of Chicxulub Impactites Recovered During IODP-ICDP Expedition 364: Large Meteorite Impacts and Planetary Evolution VI, Brasília, LPI Contribution no. 2136, abstract 5079.

Dennis, A.J., Wright, J.E., 1997. The Carolina terrane in northwestern South Carolina, USA: Late Precambrian-Cambrian deformation and metamorphism in a peri-Gondwanan oceanic arc. Tectonics, v. 16, p. 460–473.

Dickinson, W.R., Lawton, T.F., 2001. Carboniferous to Cretaceous assembly and fragmentation of Mexico. Geological Society of America Bulletin, v. 113, p. 1142–1160.

Dickinson, W.R., Lawton, T.F., 2003. Sequential intercontinental suturing as the ultimate control for Pennsylvanian Ancestral Rocky Mountains deformation. Geology, v. 31, p. 609. https://doi.org/10.1130/0091-7613(2003)031<0609:sisatu>2.0.co;2

Estrada-Carmona, J., Weber, B., Martens, U., López-Martínez, M., 2012. Petrogenesis of Ordovician magmatic rocks in the southern Chiapas Massif Complex: relations with the early Palaeozoic magmatic belts of northwestern Gondwana. International Geology Review, v. 54, p. 1918–1943.

Ganapathy, R., 1980. A major meteorite impact on the Earth 65 million years ago: Evidence from the Cretaceous-Tertiary boundary clay. Science, v. 209, p. 921–923.

Gleason, J.D., Gehrels, G.E., Dickinson, W.R., Patchett, P.J. and Kring, D.A., 2007. Laurentian sources for detrital zircon grains in turbidite and deltaic sandstones of the Pennsylvanian Haymond Formation, Marathon assemblage, west Texas, USA. Journal of Sedimentary Research, v. 77 no. 11, p. 888-900.

Grimes, C.B., Wooden, J.L., Cheadle, M.J., John, B.E., 2015. Fingerprinting tectono-magmatic provenance using trace elements in igneous zircon. Contributions to Mineralogy and

Petrology, v. 170, p. 46.

Gulick, S.P.S., Barton, P.J., Christeson, G.L., Morgan, J.V., McDonald, M., Mendoza-Cervantes, K., Pearson, Z.F., Surendra, A., Urrutia-Fucugauchi, J., Vermeesch, P.M., Warner, M.R., 2008. Importance of pre-impact crustal structure for the asymmetry of the Chicxulub impact crater. Nature Geosciences, v. 1, p. 131–135. https://doi.org/10.1038/ngeo103

Gulick, S.P., Bralower, T.J., Ormö, J., Hall, B., Grice, K., Schaefer, B., Lyons, S., Freeman, K.H., Morgan, J.V., Artemieva, N., et al., 2019. The first day of the Cenozoic. Proceedings of the National Academy of Sciences, v. 116, p. 19342–19351.

Gulick, S.P., Morgan, J., Mellett, C.L., Scientists, T.E.3., 2017. Expedition 364 Preliminary Report: Chicxulub: Drilling the K-Pg Impact Crater. doi:10.14379/iodp.pr.364.2017.

Hatcher, R.D., Jr., 2002, Alleghanian (Appalachian) orogeny, a product of zipper tectonics: Rotational transpressive continent-continent collision and closing of ancient oceans along irregular margins *in* Martínez Catalán, J.R., Hatcher, R.D., Jr., Arenas, R., and Díaz García, F., eds., Variscan-Appalachian dynamics: The building of the late Paleozoic basement: Geological Society of America Special Paper 364, p. 199–208.

Heatherington, A. L., Mueller, P. A. Nutman, A.P., 1996. Neoproterozoic magmatism in the Suwannee terrane: Implications for terrane correlation *in* Nance, R. D. & Thompson, M. D., eds., Avalonian and Related Peri-Gondwanan Terranes of the Circum-North Atlantic. Geological Society of America, Special Paper, 304, 257–268.

Heatherington A.L. Mueller P.A., 1997, Geochemistry and origin of Florida crustal basement terranes, *in* Randazzo A.F. Jones D.S., eds., The geology of Florida: Gainesville, University Press of Florida, p. 27–37.

Heatherington, A.L., Mueller, P.A., Wooden, J.L., 2010. Alleghanian plutonism in the Suwannee terrane, USA: Implications for late Paleozoic tectonic models. Geological Society of America Memoirs, v. 206, p. 607–620.

Hellstrom, J., Paton, C., Woodhead, J., Hergt, J., et al.,, 2008. Iolite: software for spatially resolved LA-(quad and MC) ICPMS analysis. Mineralogical Association of Canada Short Course Series, v. 40, p. 343–348.

Hildebrand, A.R., Penfield, G.T., Kring, D.A., Pilkington, M., Camargo Z, A., Jacobsen, S.B., Boynton, W.V., 1991. Chicxulub crater: a possible Cretaceous/Tertiary boundary impact crater on the Yucatan Peninsula, Mexico. Geology, v. 19, p. 867–871.

Hoskin, P.W., 2005. Trace-element composition of hydrothermal zircon and the alteration of Hadean zircon from the Jack Hills, Australia. Geochimica et Cosmochimica Acta, v. 69, p. 637–648.

Hoskin, P.W., Schaltegger, U., 2003. The composition of zircon and igneous and metamorphic petrogenesis. Reviews in Mineralogy and Geochemistry, v. 53, p. 27–62.

Jackson, S.E., Pearson, N.J., Griffin, W.L., Belousova, E.A., 2004. The application of laser ablation-inductively coupled plasma-mass spectrometry to in situ U--Pb zircon geochronology. Chemical Geology, v. 211, p. 47–69.

Jochum, K.P., Nohl, U., Herwig, K., Lammel, E., Stoll, B., Hofmann, A.W., 2005. GeoReM: a new geochemical database for reference materials and isotopic standards. Geostandards and Geoanalytical Research, v. 29, p. 333–338.

Juárez-Zúñiga, S., Solari, L.A. and Ortega-Obregón, C., 2019. Ordovician to Silurian igneous rocks in southern Mexico and Central America: geochronologic and isotopic constraints on paleogeographic models. Journal of South American Earth Sciences, v. 93, p.462-479.

Kamo, S.L., Krogh, T.E., 1995. Chicxulub crater source for shocked zircon crystals from the

Cretaceous-Tertiary boundary layer, Saskatchewan: Evidence from new U-Pb data. Geology, v. 23, p. 281–284.

Kamo, S.L., Lana, C., Morgan, J.V., 2011. U--Pb ages of shocked zircon grains link distal K--Pg boundary sites in Spain and Italy with the Chicxulub impact. Earth and Planetary Science Letters, v. 310, p. 401–408.

Kent, A.J., 2008. Lead isotope homogeneity of NIST SRM 610 and 612 glass reference materials: Constraints from laser ablation multicollector ICP-MS (LA-MC-ICP-MS) analysis. Geostandards and Geoanalytical Research, v. 32, p. 129–147.

Keppie, D.F., Keppie, J.D., 2014. The Yucatan, a Laurentian or Gondwanan fragment? Geophysical and palinspastic constraints. International Journal of Earth Sciences, v. 103, p. 1501–1512.

Keppie, J.D., Dostal, J., Murphy, J.B., Nance, R.D., 2008. Synthesis and tectonic interpretation of the westernmost Paleozoic Variscan orogen in southern Mexico: From rifted Rheic margin to active Pacific margin. Tectonophysics, v. 461, p. 277–290. https://doi.org/10.1016/j.tecto.2008.01.012

Keppie, J.D., Dostal, J., Nance, R.D., Miller, B.V., Ortega-Rivera, A., Lee, J.K., 2006. Circa 546 Ma plume-related dykes in the~ 1 Ga Novillo Gneiss (east-central Mexico): Evidence for the initial separation of Avalonia. Precambrian Research, v. 147, p. 342–353.

Keppie, J.D., Dostal, J., Norman, M., Urrutia-Fucugauchi, J., Grajales-Nishimura, M., 2011. Study of melt and a clast of 546 Ma magmatic arc rocks in the 65 Ma Chicxulub bolide breccia, northern Maya Block, Mexico: western limit of Ediacaran arc peripheral to northern Gondwana. International Geology Review, v. 53, p. 1180–1193.

Keppie, J.D., Dostal, J., Ortega-Gutiérrez, F., Lopez, R., 2001. A Grenvillian arc on the margin of Amazonia: evidence from the southern Oaxacan Complex, southern Mexico. Precambrian Research, v. 112, p. 165–181.

Keppie, J.D., Dostal, J., 2007. Rift-related basalts in the 1.2--1.3 Ga granulites of the northern Oaxacan Complex, southern Mexico: evidence for a rifted arc on the northwestern margin of Amazonia. Proceedings of the Geologists' Association, v. 118, p. 63–74.

Keppie, J.D., Nance, R.D., Dostal, J., Lee, J., Ortega-Rivera, A., 2012. Constraints on the subduction erosion/extrusion cycle in the Paleozoic Acatlán Complex of southern Mexico: geochemistry and geochronology of the type Piaxtla Suite. Gondwana Research, v. 21, p. 1050–1065.

Keppie, J.D., Nance, R.D., Murphy, J.B., Dostal, J., 2003. Tethyan, Mediterranean, and Pacific analogues for the Neoproterozoic--Paleozoic birth and development of peri-Gondwanan terranes and their transfer to Laurentia and Laurussia. Tectonophysics, v. 365, p. 195–219.

Keppie, J.D., Ortega-Gutiérrez, F., 2010. 1.3--0.9 Ga Oaxaquia (Mexico): remnant of an arc/backarc on the northern margin of Amazonia. Journal of South American Earth Sciences, v. 29, p. 21–27.

Kettrup, B., Deutsch, A., Ostermann, M., Agrinier, P., 2000. Chicxulub impactites: Geochemical clues to the precursor rocks. Meteoritics and Planetary Science, v. 35, p. 1229–1238.

Kettrup, B. and Deutsch, A., 2003. Geochemical variability of the Yucatán basement: Constraints from crystalline clasts in Chicxulub impactites. Meteoritics and Planetary Science, v. 38, no.7, p. 1079-1092.

Kirsch, M., Keppie, J.D., Murphy, J.B. and Lee, J.K., 2013. Arc plutonism in a transtensional regime: the late Palaeozoic Totoltepec pluton, Acatlán Complex, southern Mexico.

International Geology Review, v. 55, no. 3, p. 263-286.

Kring, D.A., 2005. Hypervelocity collisions into continental crust composed of sediments and an underlying crystalline basement: comparing the Ries (~ 24 km) and Chicxulub (~ 180 km) impact craters. Chemie der Erde - Geochemistry, v. 65, p. 1–46.

Kring, D.A., 2007. The Chicxulub impact event and its environmental consequences at the Cretaceous-Tertiary boundary. Palaeogeography, Palaeoclimatology, Palaeoecology, v. 255, p. 4–21.

Kring, D.A., 1995. The dimensions of the Chicxulub impact crater and impact melt sheet. Journal of Geophysical Research: Planets, v. 100, p. 16979–16986.

Kring, D.A., and Boynton, W.V., 1992. Petrogenesis of an augite-bearing melt rock in the Chicxulub structure and its relationship to K/T impact spherules in Haiti. Nature, v. 358, p. 141–144.

Kring, D.A., and Durda, D.D., 2002. Trajectories and distribution of material ejected from the Chicxulub impact crater: Implications for postimpact wildfires. Journal of Geophysical Research, 107(E8), 5062, p. 22, doi:10.1029/2001JE1532.

Kring, D.A., Tikoo, S.M., Schmieder, M., Riller, U., Rebolledo-Vieyra, M., Simpson, S.L., Osinski, G.R., Gattacceca, J., Wittmann, A., Verhagen, C.M. and Cockell, C.S., 2020. Probing the hydrothermal system of the Chicxulub impact crater. Science Advances, v. 6 no. 22, p.eaaz3053.

Krogh, T.E., Kamo, S.L., Bohor, B.A., 1993a. Fingerprinting the K/T impact site and determining the time of impact by U-Pb dating of single shocked zircons from distal ejecta. Earth and Planetary Science Letters, v. 119, p. 425–429.

Krogh, T.E., Kamo, S.L., Sharpton, V.L., Marin, L.E., Hildebrand, A.R., 1993b. U-Pb ages of single shocked zircons linking distal K/T ejecta to the Chicxulub crater. Nature 366, 731.

Kyte, F.T., Zhou, Z., Wasson, J.T., 1980. Siderophile-enriched sediments from the Cretaceous--Tertiary boundary. Nature, v. 288, p. 651–656.

Lawlor, P.J., Ortega-Gutiérrez, F., Cameron, K.L., Ochoa-Camarillo, H., Lopez, R., Sampson, D.E., 1999. U--Pb geochronology, geochemistry, and provenance of the Grenvillian Huiznopala Gneiss of Eastern Mexico. Precambrian Research, v. 94, p. 73–99.

Liu, L. and Stockli, D.F., 2020. U-Pb ages of detrital zircons in lower Permian sandstone and siltstone of the Permian Basin, west Texas, USA: Evidence of dominant Gondwanan and peri-Gondwanan sediment input to Laurentia. Geological Society of America Bulletin, v. 132(1-2), p. 245-262.

Lopez, R., 1997. The pre-Jurassic geotectonic evolution of the Coahuila terrane, northwestern Mexico: Grenville basement, a late Paleozoic arc, Triassic plutonism, and the events south of the Ouachita suture, Ph.D. Dissertation, Santa Cruz, California, University of California, pp. 55– 147.

Lopez, R., Cameron, K.L., Jones, N.W., 2001. Evidence for Paleoproterozoic, Grenvillian, and Pan-African age Gondwanan crust beneath northeastern Mexico. Precambrian Research, v. 107, p. 195–214.

Lopez Ramos, E., 1975. Geological summary of the Yucatan Peninsula, in: The Gulf of Mexico and the Caribbean. Springer, p. 257–282.

Mann, P., Rogers, R.D., Gahagan, L., 2007. Overview of Plate Tectonic History and Its Unresolved Tectonic Problems. Central America: Geology, Resources and Hazards, v. 1, p. 201–237.

Marsh, J.H., Stockli, D.F., 2015. Zircon U--Pb and trace element zoning characteristics in an anatectic granulite domain: Insights from LASS-ICP-MS depth profiling. Lithos, v. 239, p. 170–185.

Marshall, R.H., 1974. Petrology of the subsurface Mesozoic rocks of the Yucatan platform. Mexico [MS thesis]: New Orleans, Louisiana, University of New Orleans.

Martens, U., Weber, B., Valencia, V.A., 2010. U/Pb geochronology of Devonian and older Paleozoic beds in the southeastern Maya Block, Central America: Its affinity with peri-Gondwanan terranes. Geological Society of America Bulletin, v. 122, p. 815–829.

Marton, G., Buffler, R.T., 1994. Jurassic reconstruction of the Gulf of Mexico Basin. International Geology Review, v. 36, p. 545–586.

McDonough, W.F., Sun, S.-S., 1995. The composition of the Earth. Chemical Geology, v. 120, p. 223–253.

McKee, J.W., Jones, N.W., and Anderson, T.H., 1999, The late Paleozoic and early Mesozoic history of the Las Delicias terrane, Coahuila, Mexico *in* Bartolini, C., et al., eds., Mesozoic sedimentary and tectonic history of north-central Mexico: Geological Society of America Special Paper 340 , p. 161–189.

Middleton, M., Keppie, J.D., Murphy, J.M., Miller, B.V., and Nance, R.D., 2007, P-T-t constraints on exhumation following subduction in the Rheic Ocean: Eclogitic Asis Lithodeme, Piaxtle Suite, Acatlán Complex, southern Mexico, *in* Linnemann, U., Nance, R.D., Kraft, P., and Zulauf, G., eds., The evolution of the Rheic Ocean: From Avalonian-Cadomian active margin to Alleghenian-Variscan collision: Geological Society of America Special Paper 423, p. 489–509.

Miller, B.V., Dostal, J., Keppie, J.D., Nance, R.D., Ortega-Rivera, A. and Lee, J.K., 2007. Ordovician calc-alkaline granitoids in the Acatlán Complex, southern México:

Geochemical and geochronologic data and implications for the tectonics of the Gondwanan margin of the Rheic Ocean *in* Linnemann, U., Nance, R.D., Kraft, P., and Zulauf, G., eds., The evolution of the Rheic Ocean: From Avalonian-Cadomian active margin to Alleghenian-Variscan collision: Boulder, Colorado, Geological Society of America Special Paper 423, p. 465. doi: 10.1130/2007.2423.

Morgan, J.V., Gulick, S.P., Bralower, T., Chenot, E., Christeson, G., Claeys, P., Cockell, C., Collins, G.S., Coolen, M.J., Ferrière, L., et al., 2016. The formation of peak rings in large impact craters. Science, v. 354, p. 878–882.

Morgan, J.V., Gulick, S.P.S., et al., 2017, Chicxulub: Drilling the K-Pg Impact Crater, *in* Proceedings of the International Ocean Discovery Program, Volume 364: College Station, Texas. doi:10.14379/iodp.proc.364.2017

Mueller, P.A., Heatherington, A.L., Foster, D.A., Thomas, W.A., Wooden, J.L., 2014. The Suwannee suture: Significance for Gondwana-Laurentia terrane transfer and formation of Pangaea. Gondwana Research, v. 26, p. 365–373.

Nance, R.D., Gutiérrez-Alonso, G., Keppie, J.D., Linnemann, U., Murphy, J.B., Quesada, C., Strachan, R.A., Woodcock, N.H., 2012. A brief history of the Rheic Ocean. Geoscience Frontiers, v. 3, p. 125–135. https://doi.org/10.1016/j.gsf.2011.11.008

Nance, R.D., Linnemann, U., 2008. The Rheic Ocean: origin, evolution, and significance. GSA Today, v. 18, p. 4–12.

Nance, R.D., Miller, B.V., Keppie, J.D., Murphy, J.B., Dostal, J., 2007. Vestige of the Rheic ocean in North America: the Acatlán complex of southern Mexico *in* Linnemann, U., Nance, R.D., Kraft, P., and Zulauf, G., eds., The evolution of the Rheic Ocean: From Avalonian-Cadomian active margin to Alleghenian-Variscan collision: Boulder, Colorado, Geological Society of America Special Paper 423, p. 437.

Nance, R.D., Miller, B.V., Keppie, J.D., Murphy, J.B., Dostal, J., 2006. Acatlán Complex, southern Mexico: Record spanning the assembly and breakup of Pangea. Geology, v. 34, p. 857. https://doi.org/10.1130/g22642.1

Ortega-Gutierrez, F., Ruiz, J., Centeno-Garcia, E., 1995. Oaxaquia, a Proterozoic microcontinent accreted to North America during the late Paleozoic. Geology, v. 23, p. 1127–1130.

Ortega-Gutiérrez, F., Elías-Herrera, M., Morán-Zenteno, D.J., Solari, L., Weber, B., Luna-González, L., 2018. The pre-Mesozoic metamorphic basement of Mexico, 1.5 billion years of crustal evolution. Earth-Science Reviews, v. 183, p. 2–37.

Ortega-Obregón, C., Keppie, J.D., Solari, L.A., Ortega-Gutiérrez, F., Dostal, J., Lopez, R., Ortega-Rivera, A., Lee, J., 2003. Geochronology and geochemistry of the~ 917 Ma, calc-alkaline Etla granitoid pluton (Oaxaca, southern Mexico): Evidence of post-Grenvillian subduction along the northern margin of Amazonia. International Geology Review, v. 45, p. 596–610.

Ortega-Obregon, C., Keppie, J.D., Murphy, J.B., Lee, J.K.W., Ortega-Rivera, A., 2009. Geology and geochronology of Paleozoic rocks in western Acatlán Complex, southern Mexico: Evidence for contiguity across an extruded high-pressure belt and constraints on Paleozoic reconstructions. Geological Society of America Bulletin, v. 121, p. 1678–1694. https://doi.org/10.1130/b26597.1

Ortega-Obregón, C., Solari, L., Gómez-Tuena, A., Elías-Herrera, M., Ortega-Gutiérrez, F., Macías-Romo, C., 2014. Permian--Carboniferous arc magmatism in southern Mexico: U--Pb dating, trace element and Hf isotopic evidence on zircons of earliest subduction beneath the western margin of Gondwana. International Journal of Earth Sciences, v. 103,

p. 1287–1300.

Paton, C., Hellstrom, J., Paul, B., Woodhead, J., Hergt, J., 2011. Iolite: Freeware for the visualisation and processing of mass spectrometric data. Journal of Analytical Atomic Spectrometry, v. 26, p. 2508–2518.

Petrus, J.A., Kamber, B.S., 2012. VizualAge: A novel approach to laser ablation ICP-MS U-Pb geochronology data reduction. Geostandards and Geoanalytical Research, v. 36, no. 2 p. 47–270.

Pindell, J., Dewey, J.F., 1982. Permo-Triassic reconstruction of western Pangea and the evolution of the Gulf of Mexico/Caribbean region. Tectonics v. 1, p. 179–211.

Pindell, J.L., 1985. Alleghenian reconstruction and subsequent evolution of the Gulf of Mexico, Bahamas, and Proto-Caribbean. Tectonics, v. 4, no. 1, p.1-39.

Pindell, J.L., Cande, S.C., Pitman, W.C., III, Rowley, D.B., Dewey, J.F., LaBrecque, J., Haxby, W., 1988. A plate-kinematic framework for models of Caribbean evolution. Tectonophysics, v. 155, p. 121–138.

Pindell, J.L., Kennan, L., 2009. Tectonic evolution of the Gulf of Mexico, Caribbean and northern South America in the mantle reference frame: an update. Geological Society, London, Special Publications, v. 328, p. 1–55.

Pindell, J.L., Kennan, L., Barrett, S., 2000. Putting it all together again. AAPG Explorer, v. 21, p. 58–62.

Poppe, S., Galland, O., de Winter, N.J., Goderis, S., Claeys, Ph., Debaille, V., Boulvais, P., and Kervyn, M., 2020, Structural and Geochemical Interactions Between Magma and Sedimentary Host Rock: the Hovedøya Case, Oslo Rift, Norway: Geochemistry, Geophysics, Geosystems, v. 21 no. 3, e2019GC008685. doi:10.1029/2019gc008685

Premo, W.R. and Izett, G.A., 1993. U-Pb provenance ages of shocked zircons from the KT boundary, Raton basin, Colorado. Lunar and Planetary Science Conference. 24, abstract no. 1171.

Rae, A.S., Collins, G.S., Poelchau, M., Riller, U., Davison, T.M., Grieve, R.A., Osinski, G.R., Morgan, J.V., Expedition, I.-I., 2019. Stress-Strain Evolution During Peak-Ring Formation: A Case Study of the Chicxulub Impact Structure. Journal of Geophysical Research: Planets, v. 124, p. 396–417.

Rasmussen, C., Stockli, D.F., Ross, C.H., Pickersgill, A., Gulick, S.P., Schmieder, M., Christeson, G.L., Wittmann, A., Kring, D.A., Morgan, J.V., et al., 2019. U-Pb memory behavior in Chicxulub's peak ring—Applying U-Pb depth profiling to shocked zircon. Chemical Geology, v. 525, p. 356–367.

Rasmussen, C., Stockli, D. F., Erickson, T. M., and Schmieder, M., 2020. Spatial U-Pb age distribution in shock-recrystallized zircon–A case study from the Rochechouart impact structure, France. Geochimica et Cosmochimica Acta, v. 273, p. 313-330.

Reiners, P.W., 2005. Zircon (U-Th)/He thermochronometry. Reviews in Mineralogy and Geochemistry, v. 58 no. 1, p.151-179.

Riller, U., Poelchau, M.H., Rae, A.S., Schulte, F.M., Collins, G.S., Melosh, H.J., Grieve, R.A., Morgan, J.V., Gulick, S.P., Lofi, J., et al., 2018. Rock fluidization during peak-ring formation of large impact structures. Nature, v. 562, p. 511–519.

Ross, M.I., Scotese, C.R., 1988. A hierarchical tectonic model of the Gulf of Mexico and Caribbean region. Tectonophysics, v. 155, p. 139–168.

Rubatto, D., 2002. Zircon trace element geochemistry: partitioning with garnet and the link between U-Pb ages and metamorphism. Chemical Geology, v. 184, p. 123–138.

Ruiz, J., Tosdal, R.M., Restrepo, P.A., and Murillo-Muñetón, G., 1999, Pb isotope evidence for Colombia–southern Mexico connections in the Proterozoic *in* Ramos, V.A., and Keppie, J.D., eds., Laurentia-Gondwana connections before Pangea: Geological Society of America Special Paper 336 , p. 183–197.

Samson, S.D., 2001. Timing of Alleghanian magmatism revisited, in: Geological Society of America Abstracts with Programs, v. 33 p. 7.

Schaaf, G., Ernst, P., Weber, B., Weis, P., Groß, A., Ortega-Gutiérrez, F., Köhler, H., 2002. The Chiapas Massif (Mexico) revised: New geologic and isotopic data and basement characteristics. Neues Jahrbuch fur Geologie und Palaontologie-Abhandlungen, v. 225, p. 1–23.

Schmieder, M., Kring, D.A., Lapen, T.J., Gulick, S., Stockli, D.F., Rasmussen, C., Rae, A., Ferrière, L., Poelchau, M., Xiao, L., et al., 2017. Sphene and TiO2 Assemblages in the Chicxulub Peak Ring: U-Pb Systematics and Implications for Shock Pressures, Temperatures, and Crater Cooling. Annual Meeting of the Meteoritical Society 1987, abstract 6134.

Schmieder, M., Shaulis, B.J., Lapen, T.J., Kring, D.A., 2018. U--Th--Pb systematics in zircon and apatite from the Chicxulub impact crater, Yucatán, Mexico. Geological Magazine, v. 155, p. 1330–1350.

Schoene, B., 2014. 4.10-U–Th–Pb Geochronology. Treatise on geochemistry, v. 4, p. 341-378.

Schulte, P., Alegret, L., Arenillas, I., Arz, J.A., Barton, P.J., Bown, P.R., Bralower, T.J., Christeson, G.L., Claeys, P., Cockell, C.S., et al., 2010. The Chicxulub asteroid impact and mass extinction at the Cretaceous-Paleogene boundary. Science, v. 327, p. 1214–1218.

Seton, M., Müller, R.D., Zahirovic, S., Gaina, C., Torsvik, T., Shephard, G., Talsma, A., Gurnis, M., Turner, M., Maus, S., et al., 2012. Global continental and ocean basin reconstructions since 200 Ma. Earth-Science Reviews, v. 113, p. 212–270.

Shaulis, B.J., Lapen, T.J., Casey, J.F. and Reid, D.R., 2012. Timing and rates of flysch sedimentation in the Stanley Group, Ouachita Mountains, Oklahoma and Arkansas, USA: Constraints from U-Pb zircon ages of subaqueous ash-flow tuffs. Journal of Sedimentary Research, v. 82 no. 11, p. 833-840.

Sláma, J., Košler, J., Condon, D.J., Crowley, J.L., Gerdes, A., Hanchar, J.M., Horstwood, M.S., Morris, G.A., Nasdala, L., Norberg, N., et al., 2008. Plešovice zircon—a new natural reference material for U--Pb and Hf isotopic microanalysis. Chemical Geology, v. 249, p. 1–35.

Soreghan, G.S. and Soreghan, M.J., 2013. Tracing Clastic Delivery to the Permian Delaware Basin, USA: Implications for Paleogeography and Circulation in Westernmost Equatorial Pangea, Tracing Clastic Dispersal to the Westernmost Pangean Suture. Journal of Sedimentary Research, v. 83, no. 9, p. 786-802.

Smit, J., 1999. The global stratigraphy of the Cretaceous-Tertiary boundary impact ejecta. Annual Review of Earth and Planetary Sciences 27, p. 75–113.

Smit, J., Hertogen, J., 1980. An extraterrestrial event at the Cretaceous--Tertiary boundary. Nature, v. 285, p. 198–200.

Solari, L.A., Keppie, J.D., Gutiérrez, F.O., Cameron, K.L., Lopez, R., 2004a. 990 Ma peak granulitic metamorphism and amalgamation of Oaxaquia, Mexico: U Pb zircon geochronological and common Pb isotopic data. Revista Mexicana de Ciencias Geológicas, v. 21, p. 212–225.

Solari, L.A., Keppie, J.D., Ortega-Gutierrez, F., Ortega-Rivera, A., Hames, W.E., Lee, J., 2004b. Phanerozoic structures in the Grenvillian northern Oaxacan Complex, southern Mexico: result of thick-skinned tectonics. International Geology Review, v. 46, p. 614–628.

Solari, L.A., Ortega-Gutiérrez, F., Elías-Herrera, M., Gómez-Tuena, A., Schaaf, P., 2010. Refining the age of magmatism in the Altos Cuchumatanes, western Guatemala, by LA--ICPMS, and tectonic implications. International Geology Review, v. 52, p. 977–998.

Solari, L.A., Ortega-Gutiérrez, F., Elías-Herrera, M., Schaaf, P., Norman, M., Ortega-Obregón, C., Chiquin, M., et al., 2009. U-Pb zircon geochronology of Palaeozoic units in western and central Guatemala: Insights into the tectonic evolution of Middle America. Geological Society, London, Special Publications, v. 328, p. 295–313.

Soto-Kerans, G.M., Stockli, D.F., Janson, X., Lawton, T.F. and Covault, J.A., 2020. Orogen proximal sedimentation in the Permian foreland basin. Geosphere, v. 16, no. 2, p.567-593.

Steiner M.B., 2005, Pangean reconstruction of the Yucatan block: Its Permian, Triassic, and Jurassic geologic and tectonic history, *in* Anderson T.H. Nourse J.A. McKee J.W. Steiner M.B., eds., The Mojave-Sonora Megashear Hypothesis: Development, Assessment, and Alternatives: Geological Society of America Special Paper 393, p. 457–480.

Steiner, M.B., Walker, J.D., 1996. Late Silurian plutons in Yucatan. Journal of Geophysical Research: Solid Earth, v. 101, p. 17727–17735.

Stern, R.J., Dickinson, W.R., 2010. The Gulf of Mexico is a Jurassic back-arc basin. Geosphere, v. 6, p. 739–754.

Stewart, J.H., Blodgett, R.B., Boucot, A.J., Carter, J.L., and López, R., 1999, Exotic Paleozoic strata of Gondwanan provenance near Ciudad Victoria, Tamaulipas, Mexico *in* Ramos, V.A., and Keppie, J.D., eds., Laurentia-Gondwana connections before Pangea: Geological Society of America Special Paper 336 , p. 227–252.

Swisher, C.C., Grajales-Nishimura, J.M., Montanari, A., Margolis, S.V., Claeys, P., Alvarez, W., Renne, P., Cedillo-Pardoa, E., Maurrasse, F.J.R., Curtis, G.H. and Smit, J., 1992. Coeval $^{40}Ar/^{39}Ar$ ages of 65.0 million years ago from Chicxulub crater melt rock and Cretaceous-Tertiary boundary tektites. Science, v. 257, no. 5072, p. 954-958.

Stöffler, D., 1971. Progressive metamorphism and classification of shocked and brecciated crystalline rocks at impact craters. Journal of Geophysical Research, v. 76, p. 5541–5551.

Thomas, W.A., 2010. Interactions between the southern Appalachian–Ouachita orogenic belt and basement faults in the orogenic footwall and foreland, *in* From Rodinia to Pangea: the Lithotectonic Record of the Appalachian Region. Geological Society of America Memoirs, v. 206, p.897-916. doi:10.1130/2010.1206(34)

Thomas, W.A., Gehrels, G.E., Lawton, T.F., Satterfield, J.I., Romero, M.C., Sundell, K.E., 2019. Detrital zircons and sediment dispersal from the Coahuila terrane of northern Mexico into the Marathon foreland of the southern Midcontinent. Geosphere, v. 15, no. 4, p.1102-1127.

Timms, N.E., Kirkland, C.L., Cavosie, A.J., Rae, A.S., Rickard, W.D., Evans, N.J., Erickson, T.M., Wittmann, A., Ferrière, L., Collins, G.S. and Gulick, S.P., 2020. Shocked titanite records Chicxulub hydrothermal alteration and impact age. Geochimica et Cosmochimica Acta, v. 281, p.12-30.

Trail, D., Watson, E.B., Tailby, N.D., 2012. Ce and Eu anomalies in zircon as proxies for the oxidation state of magmas. Geochimica et Cosmochimica Acta, v. 97, p. 70–87.

Trainor, R.J., Nance, R.D., and Keppie, J.D., 2011, Tectonothermal history of the

Mesoproterozoic Novillo Gneiss of eastern Mexico: Support for coherent Oaxaquia microcontinent: Revista Mexicana de Ciencias Geológicas, v. 28, p. 580–592.

Vega-Granillo, R., Talavera-Mendoza, O., Meza-Figueroa, D., Ruiz, J., Gehrels, G.E., and López-Martínez, M., 2007, Pressure-temperature-time evolution of Paleozoic high-pressure rocks of the Acatlán Complex (southern Mexico): Implications for the evolution of the Iapetus and Rheic Oceans: Geological Society of America Bulletin, v. 119, p. 1249–1264, doi: 10.1130/B226031.1

Vermeesch, P., 2018, IsoplotR: a free and open toolbox for geochronology. Geoscience Frontiers, v. 9, p.1479-1493, doi: 10.1016/j.gsf.2018.04.001.

Viele, G.W., and Thomas, W.A., 1989, Tectonic synthesis of the Ouachita orogenic belt, *in* Hatcher, R.D., Jr., Thomas, W.A., and Viele, G.W., eds., The Appalachian-Ouachita orogen in the United States: Boulder, Colorado, The Geological Society of America, Geology of North America, v. F-2, p. 695–728.

Weber, B., Cameron, K.L., Osorio, M., Schaaf, P., 2005. A Late Permian tectonothermal event in Grenville crust of the southern Maya terrane: U-Pb zircon ages from the Chiapas Massif, southeastern Mexico. International Geology Review, v. 47, p. 509–529.

Weber, B., González-Guzmán, R., Manjarrez-Juárez, R., de León, A.C., Martens, U., Solari, L., Hecht, L., Valencia, V., 2018. Late Mesoproterozoic to Early Paleozoic history of metamorphic basement from the southeastern Chiapas Massif Complex, Mexico, and implications for the evolution of NW Gondwana. Lithos, v. 300, p. 177–199.

Weber, B., Hecht, L., 2003. Petrology and geochemistry of metaigneous rocks from a Grenvillian basement fragment in the Maya Block: the Guichicovi complex, Oaxaca, southern Mexico. Precambrian Research, v. 124, p. 41–67.

Weber, B., Köhler, H., 1999. Sm--Nd, Rb--Sr and U--Pb geochronology of a Grenville Terrane in Southern Mexico: origin and geologic history of the Guichicovi Complex. Precambrian Research, v. 96, p. 245–262.

Weber, B., Iriondo, A., Premo, W.R., Hecht, L., Schaaf, P., 2007. New insights into the history and origin of the southern Maya Block, SE México: U–Pb–SHRIMP zircon geochronology from metamorphic rocks of the Chiapas massif. International Journal of Earth Science, v. 96, p. 253–269. https://doi.org/10.1007/s00531-006-0093-7

Weber, B., Scherer, E.E., Schulze, C., Valencia, V.A., Montecinos, P., Mezger, K. and Ruiz, J., 2010. U–Pb and Lu–Hf isotope systematics of lower crust from central-southern Mexico–Geodynamic significance of Oaxaquia in a Rodinia Realm. Precambrian Research, v. 182, no. 1-2 , p.149-162.

Weber, B. and Schulze, C.H., 2014. Early Mesoproterozoic (> 1.4 Ga) ages from granulite basement inliers of SE Mexico and their implications on the Oaxaquia concept–Evidence from U-Pb and Lu-Hf isotopes on zircon. Revista Mexicana de Ciencias Geológicas, v. 31 no. 3, p.377-394.

Weber, B., Valencia, V.A., Schaaf, P., Gutiérrez, F.O., 2009. Detrital zircon ages from the Lower Santa Rosa Formation, Chiapas: implications on regional Paleozoic stratigraphy. Revista Mexicana de Ciencias Geológicas, v. 26, p. 260–276.

Weber, B., Valencia, V.A., Schaaf, P., Pompa-Mera, V., Ruiz, J., 2008. Significance of Provenance Ages from the Chiapas Massif Complex (Southeastern Mexico): Redefining the Paleozoic Basement of the Maya Block and Its Evolution in a Peri-Gondwanan Realm. The Journal of Geology, v. 116, p. 619–639. doi:10.1086/591994

Wetherill, G.W., 1956. Discordant uranium-lead ages. Eos, Transactions American Geophysical

Union, v. 37, p. 320–326.

Wiedenbeck, M., Alle, P., Corfu, F., Griffin, W.L., Meier, M., Oberli, F.V., Quadt, A.V., Roddick, J.C., Spiegel, W., 1995. Three natural zircon standards for U-Th-Pb, Lu-Hf, trace element and REE analyses. Geostandards newsletter, v. 19, p. 1–23.

Wittmann, A., Kenkmann, T., Schmitt, R. T., and Stöffler, D., 2006. Shock-metamorphosed zircon in terrestrial impact craters. Meteoritics and Planetary Science, v. 41 no. 3, p. 433-454.

Wittmann, A., van Soest, M., Hodges, K.V., Darling, J.R., Morgan, J.V., Gulick, S.P., Stockli, D., Rasmussen, C., Kring, D.A. and Schmieder, M., 2018, May. Petrology and radioisotopic ages of allanite in the peak ring of the Chicxulub impact crater: Annual meeting of the Meteoritical Society, v. 81, abstract 2067.

Xiao, L., Zhao, J.W., Liu, H.S., Xiao, Z.Y., Morgan, J., Gulick, S., Kring, D., Claeys, P. and Riller, U., and the Expedition 364 Scientists, 2017. Ages and Geochemistry of the Basement Granitoids of the Chicxulub Impact Crater: Implications for Peak Ring Formation. In Lunar and Planetary Science Conference, v. 48, abstract 1311.

Zhao, J., Xiao, L., Gulick, S.P., Morgan, J.V., Kring, D., Urrutia-Fucugauchi, J. Schmieder, M., de Graaff, S.J., Wittmann, A., Ross, C.H. and Claeys, P., 2020. Geochemistry, geochronology and petrogenesis of Maya Block granitoids and dykes from the Chicxulub Impact Crater, Gulf of México: Implications for the assembly of Pangea. Gondwana Research, v. 82, p.128-150.

1329 FIGURES

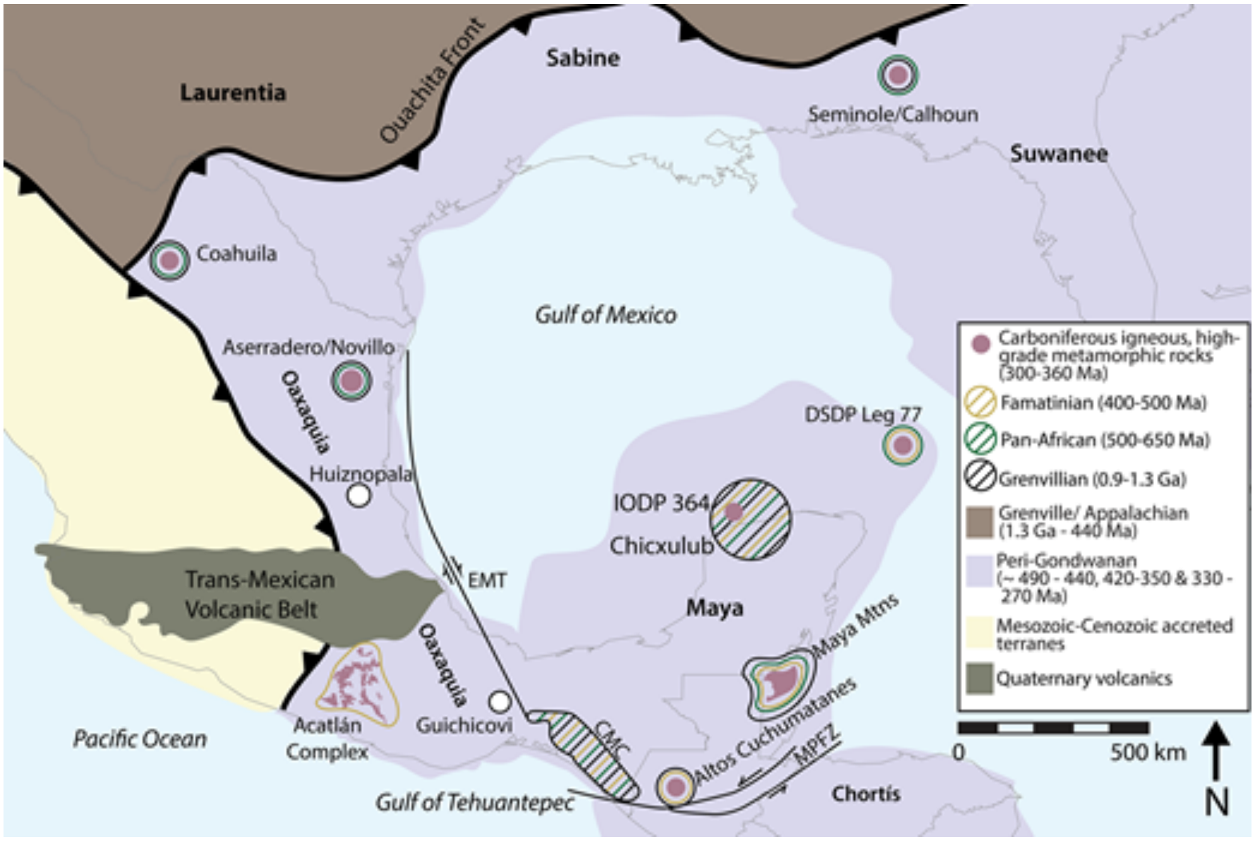

1330

1331 Figure 1. Terrane map shows the Gulf of Mexico region modified from Dickinson and Gehrels
1332 (2009); Dickinson and Lawton (2001); Gehrels et al. (2011); Lawton et al. (2015); Ortega-
1333 Gutiérrez et al. (2018); Sedlock et al. (1993); Weber et al. (2012); and references therein.
1334 Oaxaquia outcrops are shown by white dots. Suwanee and Yucatán have Gondwanan tectonic
1335 affinity. Drillcores in north Florida and south Georgia, Maya Mountains, Deep Sea Drilling
1336 Project Leg 77, Altos Cuchumatanes, Las Delicias (Coahuila), Aserradero, Acatlán Complex
1337 eclogites, Totoltepec pluton, and this study are denoted as Carboniferous arc rocks. Famatinian
1338 (400–500 Ma) related ages are circled in gold. Pan-African (500–650 Ma) ages are circled in
1339 dark green. Grenvillian (0.9–1.3 Ga) ages are circled in black. MPFZ—Motagua-Polochic Fault
1340 Zone; EMT—East Mexican Transform. Detrital zircon records, intrusion, and metamorphic
1341 cooling ages are from Alemán-Gallardo et al. (2019); Dallmeyer (1984); Estrada-Carmona et al.

(2012); Heatherington et al. (2010); Juárez-Zúñiga et al. (2019); Kirsch et al. (2013); Lopez (1997); Lopez et al. (2001); McKee et al. (1999); Middleton et al. (2007); Miller et al. (2007); Mueller et al. (2014); Ortega-Obregón et al. (2008); Schaaf et al. (2002); Solari et al. (2010); Steiner and Walker (1996); Vega-Granillo et al. (2007); Weber et al. (2005, 2007, 2009, 2012, 2018, 2019, 2020).

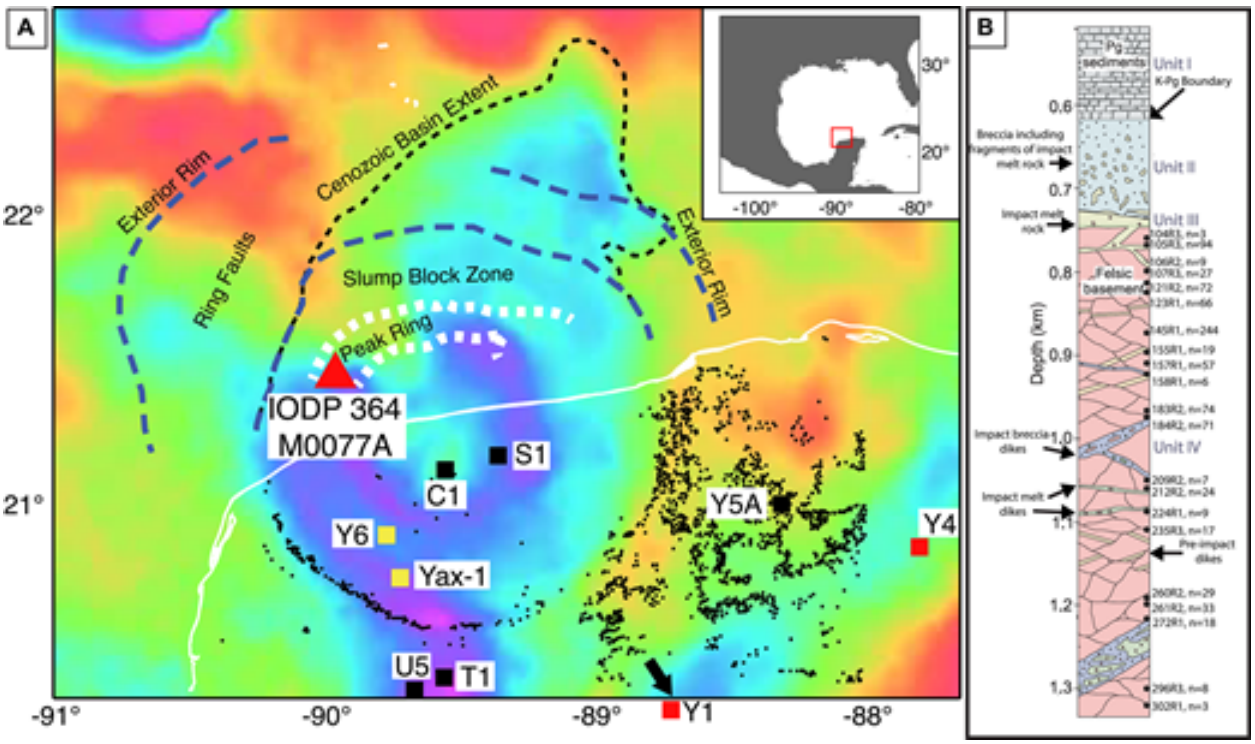

Figure 2. (A) Map shows Bouguer gravity anomaly over the Chicxulub impact structure. Thin white line is the Yucatán coastline, black squares are boreholes that recover the K-Pg section, and red squares are boreholes that penetrate Paleozoic basement. The red triangle indicates the Expedition 364 drillcore location and recovery of Paleozoic basement, which lies within the peak ring (outlined in white dashes). The black dashed line outlines the extent of the Cenozoic basin, while the blue dashed line marks the slump block zone and region containing ring faults. Black dots indicate sinkhole and denote locations from Connors et al. (1996). Red box in the inset

shows the location of the gravity anomaly map. Modified from Gulick et al. (2013). (B) Lithology from Expedition 364 from 600 m to 1.3 km below the seafloor with sample locations (black dots) and zircon yield (n); Unit I: Paleogene sediments (gray), Unit II: suevite (blue), Unit III: impact melt rock (green), Unit IV: felsic basement (pink), and pre-impact dikes (yellow). Modified from Morgan et al. (2016).

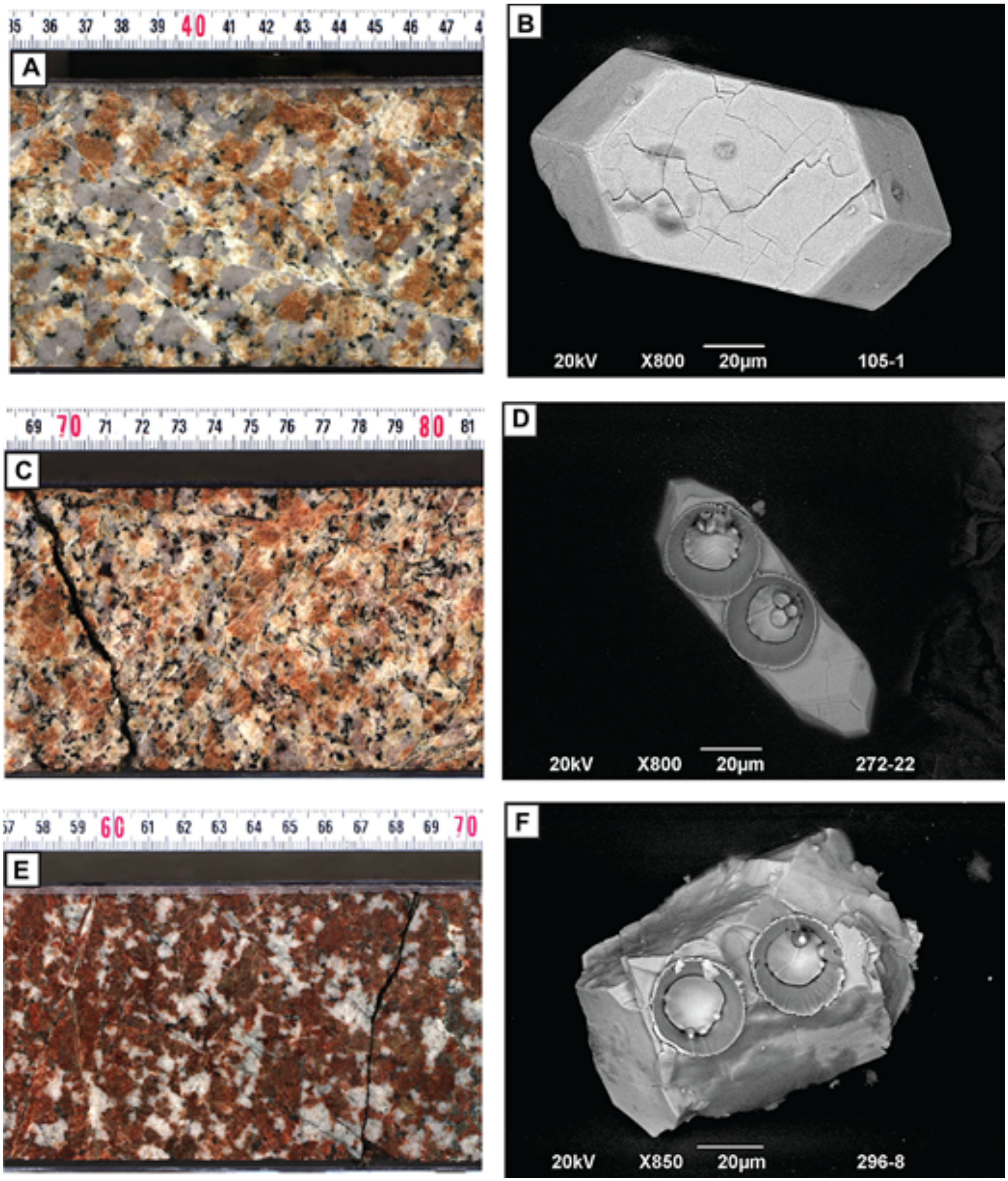

Figure 3. Various granitoid samples from the Expedition 364 core are shown. (A) Halfcore photograph of a coarse-grained granite with 1 cm translucent quartz crystals (97R3, ~752 meters below seafloor [mbsf]). (B) Zircon crystal (sample 105R3, ~772 mbsf) recovered from a granite

similar to (A). (C) Halfcore photograph of altered granite with pink quartz (272R1, ~1237 mbsf). (D) Zircon crystal recovered from the same section as (C) that displays fracturing near the edges of the crystal. The two spots on the crystal are from the laser ablation-inductively coupled plasma-mass spectrometry U-Pb and trace element analysis. (E) Halfcore photograph of red alkali-feldspar granite mainly recovered in the lowermost part of the core (296R2). The crystal exterior shows minor fracturing. (F) Zircon crystal (296R3, ~1310 mbsf) recovered from a granite similar to (E) that has a unique morphology and does not display the tetragonal crystal habit typical of zircon. Halfcore photographs from Gulick et al. (2017).

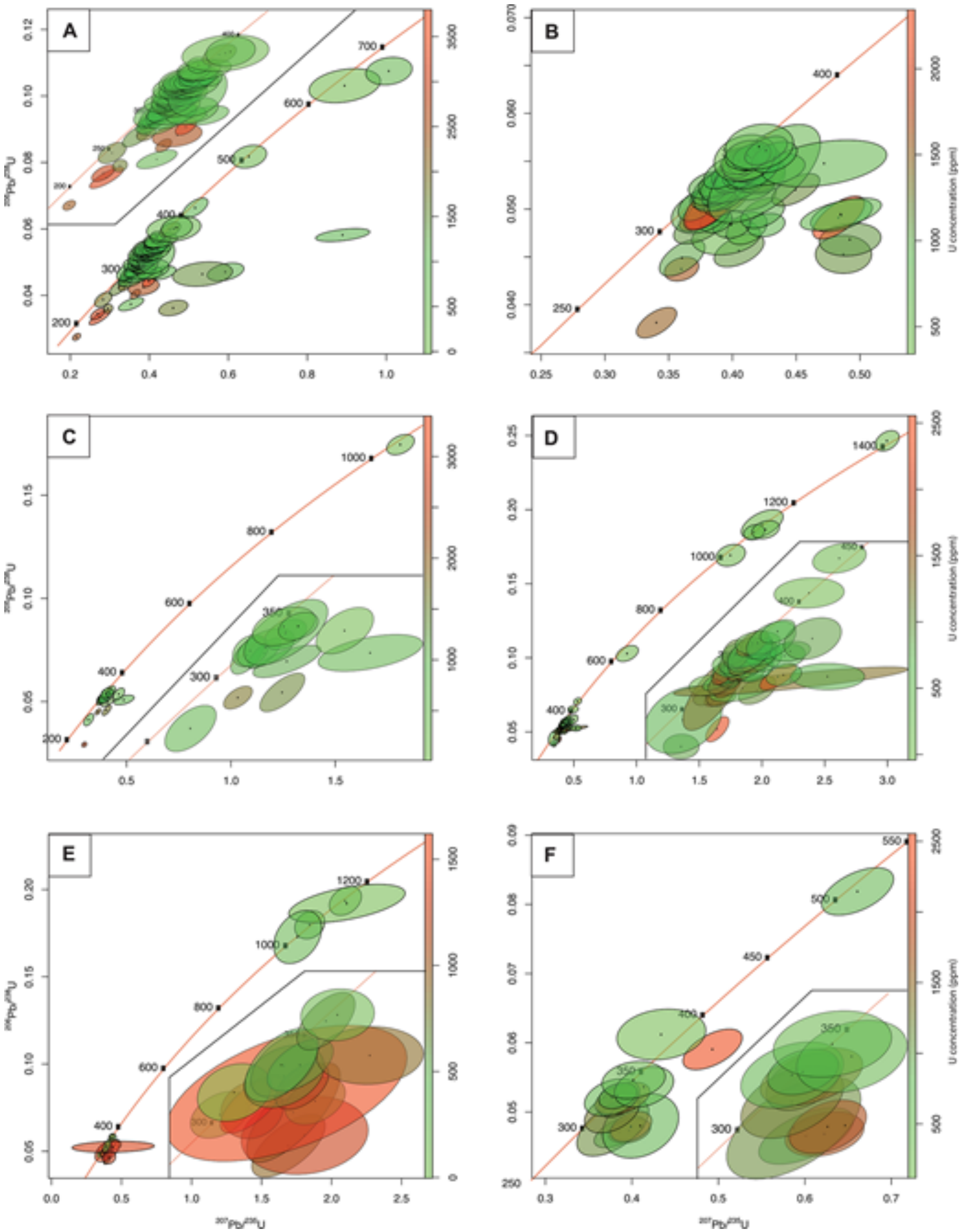
A
B
C
D
E
F
206Pb/238U
207Pb/235U
U concentration (ppm)

Figure 4. Zircon U-Pb results are plotted on Wetherill Concordia diagrams; insets show Carboniferous crystals only from six samples: (A) 105R3, (B) 123R1, (C) 155R1, (D) 184R2, (E) 212R2, and (F) 272R1. Ellipses are color-coded by U concentration (ppm) and are <30% discordant.

1378

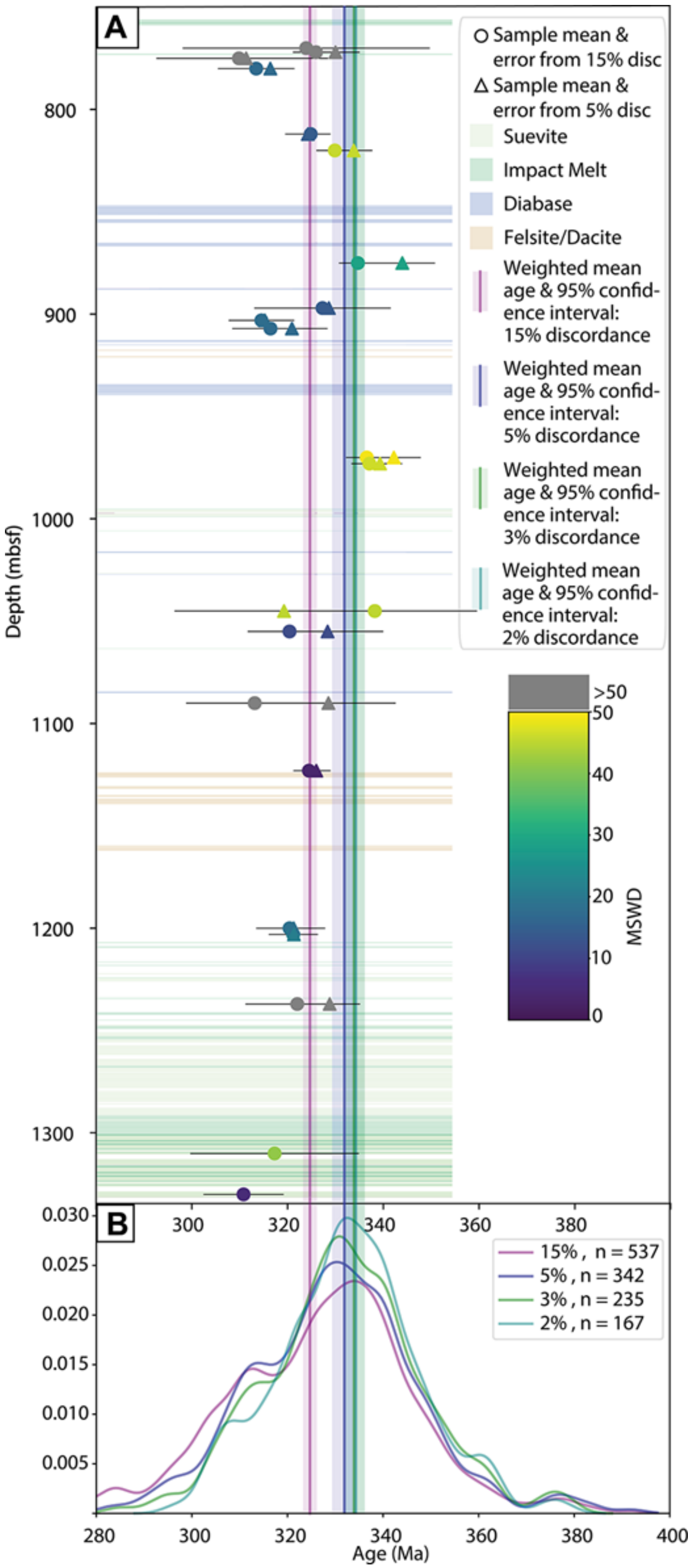

A
Sample mean & error from 15% disc
Sample mean & error from 5% disc
Suevite
Impact Melt
Diabase
Felsite/Dacite
Weighted mean age & 95% confidence interval: 15% discordance
Weighted mean age & 95% confidence interval: 5% discordance
Weighted mean age & 95% confidence interval: 3% discordance
Weighted mean age & 95% confidence interval: 2% discordance
Depth (mbsf)
800
900
1000
1100
1200
1300
>50
50
40
30
20
10
0
MSWD
B
15% , n = 537
5% , n = 342
3% , n = 235
2% , n = 167
0.030
0.025
0.020
0.015
0.010
0.005
280
300
320
340
360
380
400
Age (Ma)

Figure 5. (A) Weighted sample mean ages were sorted by depth using grains that passed the 15% discordance (circles) and 5% discordance (triangles); filters are colored by mean square of weighted deviates (MSWD). Uncertainty (black lines) reported is in the 95% confidence interval. Translucent horizontal color bars show the locations of suevite and impact melt (greens), diabase (blue), and felsite/dacite (tan). Vertical lines and associated translucent color bars are the weighted mean ages, and 95% confidence intervals were calculated using all data less than 400 Ma from all samples for all grains that passed the 15% (purple), 5% (blue), 3% (green), and 2% (teal) discordance filters. (B). Kernel Density Estimation (KDE) plots for all grains from all samples that passed the 15% (purple), 5% (blue), 3% (green), and 2% (teal) discordance filters. Vertical lines and associated translucent color bars are the same as in (A).

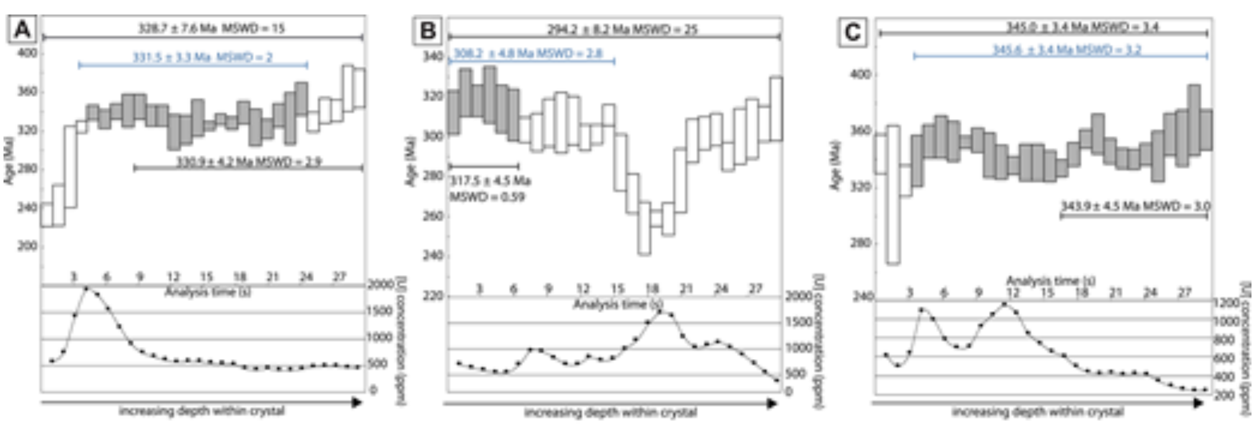

Figure 6. (A–C) Three examples (105R3#8, 105R3#7, and 145R1#45) of incremental U-Pb ages are shown. Each bar shows the 2σ error of each second of analysis. Gray bars and associated calculated ages are the preferred plateau ages used in our study. U concentration is plotted with depth within the single zircon crystal. Conventional U-Pb ages, where the age is integrated over the total analysis, are shown at the top of the plots. U-Pb plateau ages (blue) are calculated over the portion of the total analysis that excludes zones of Pb loss and inheritance where the 2σ error

of each incremental U-Pb age overlaps. The ages below the incremental U-Pb age spectra are calculated only using the incremental U-Pb data where the U concentration is <1000 ppm. MSWD—mean square of weighted deviates.

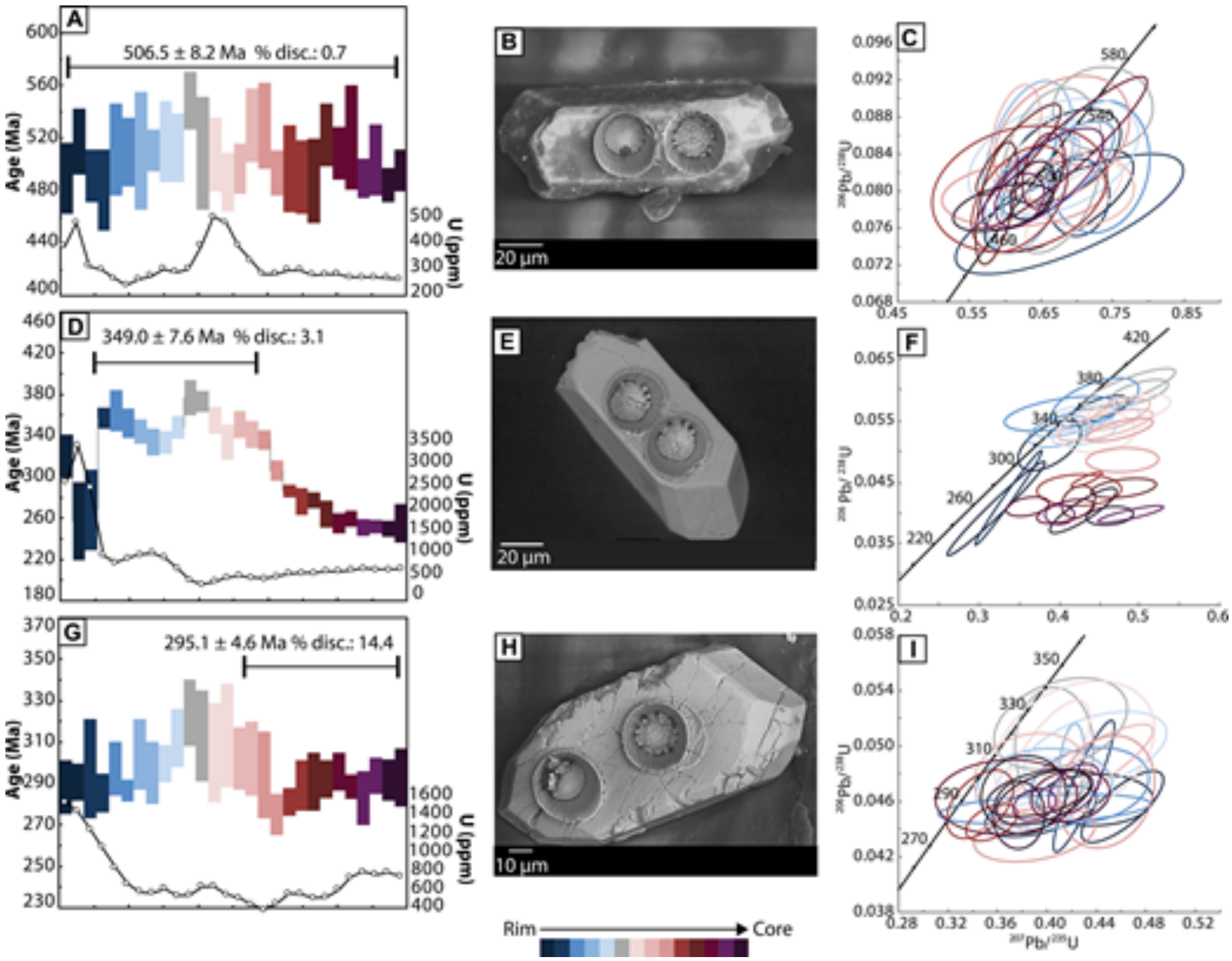

Figure 7. The following are shown from left to right columns: incremental $^{206}Pb/^{238}U$ ages through a depth-profiled crystal using internal errors and ages associated with the U-Pb plateau ages, scanning electron microscope images of the zircon crystal analyzed, and Wetherill Concordia diagrams of 1 s increments through a single crystal. (A–C) Shown are 1s increment data for an inherited Peri-Gondwanan crystal (105R3#72); (D–F) 1 s increment data for a Carboniferous zircon crystal in pristine condition externally (145R1#22); (G–I) 1 s increment data for a highly fractured Carboniferous zircon crystal (105R3#1).

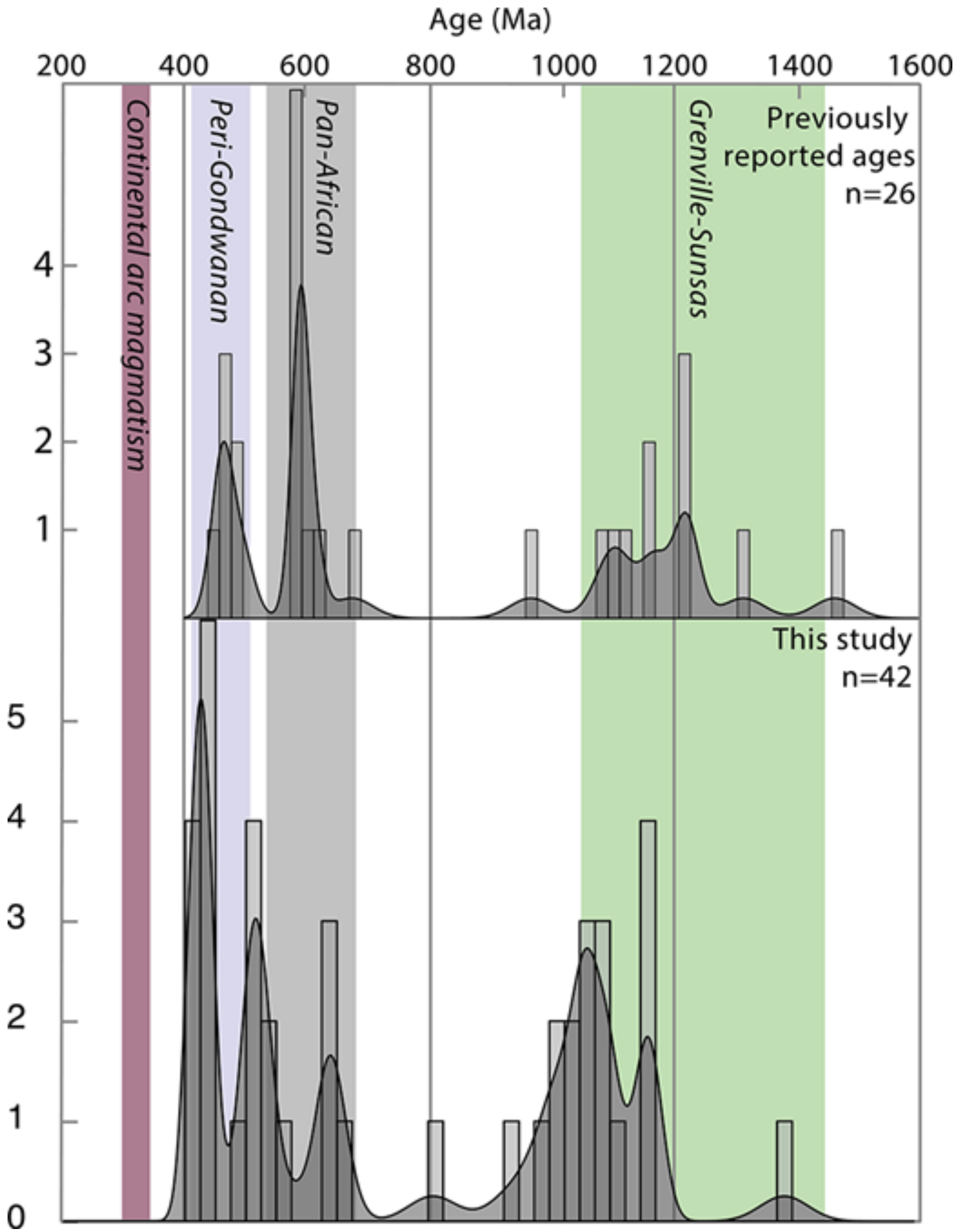

Age (Ma)
200
400
600
800
1000
1200
1400
1600
Continental arc magmatism
Peri-Gondwanan
Pan-African
Grenville-Sunsas
Previously reported ages n=26
This study n=42
4
3
2
1
5
4
3
2
1
0

Figure 8. Two kernel density estimate plots show the inherited age components. Top: Ages for the Yucatán basement from previous studies using zircon U-Pb, melt T_{CHUR}, and T_{Nd} ages. See Appendix I for ages and literature sources. Bottom: Inherited ages from International Ocean Discovery Program Expedition 364 granite. See Appendix II for raw data and sample locations. Green bar from 1.0 Ga to 1.3 Ga denotes age of Grenvillian orogeny. Gray bar from 500 Ma to 650 Ma marks the Pan-African orogeny. Light purple denotes Peri-Gondwanan terranes (ca. 400–440 Ma). Purple bar signifies the dominant Carboniferous (ca. 320–340 Ma) age component of this study.

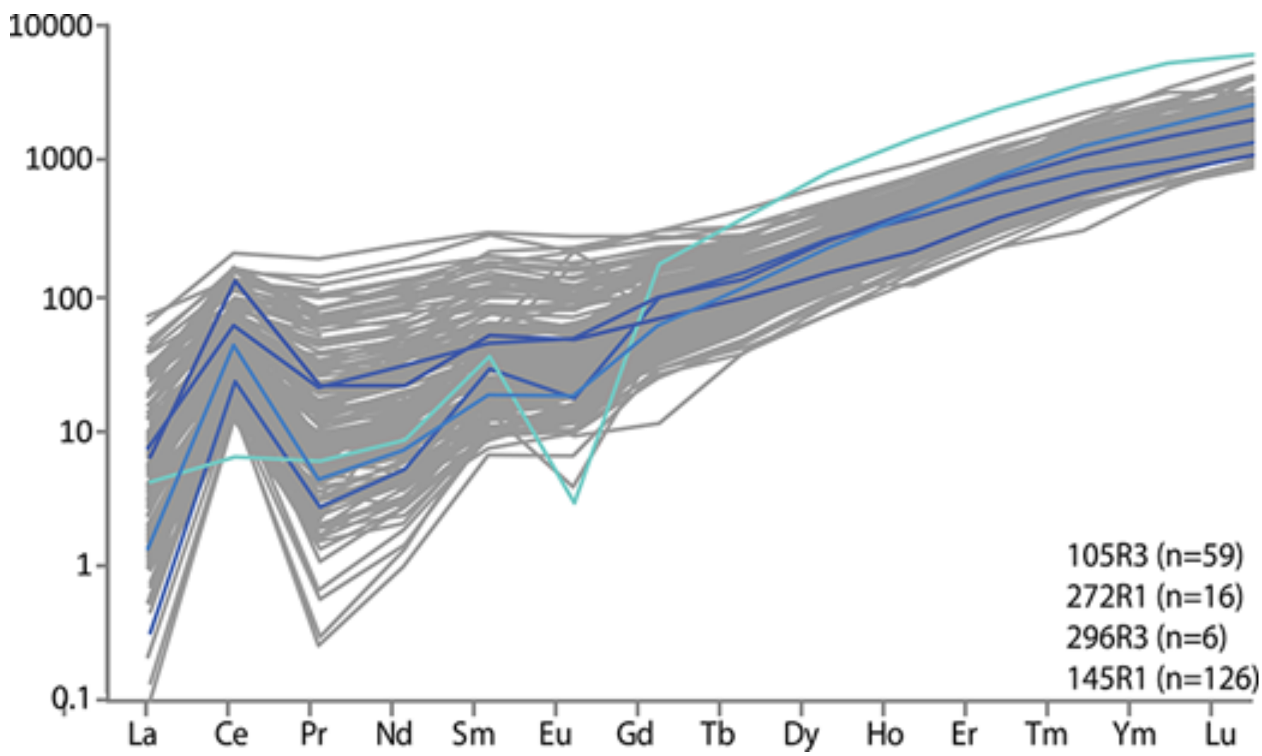

Figure 9. Measured rare earth element (REE) concentrations normalized to chondrite values are plotted (McDonough and Sun, 1995). REE values of four small samples (105R3, 145R1, 272R1, and 296R3) are plotted together. Blue lines are inherited grains (600–500 Ma) and teal line is an inherited grain with age between 500–400 Ma.

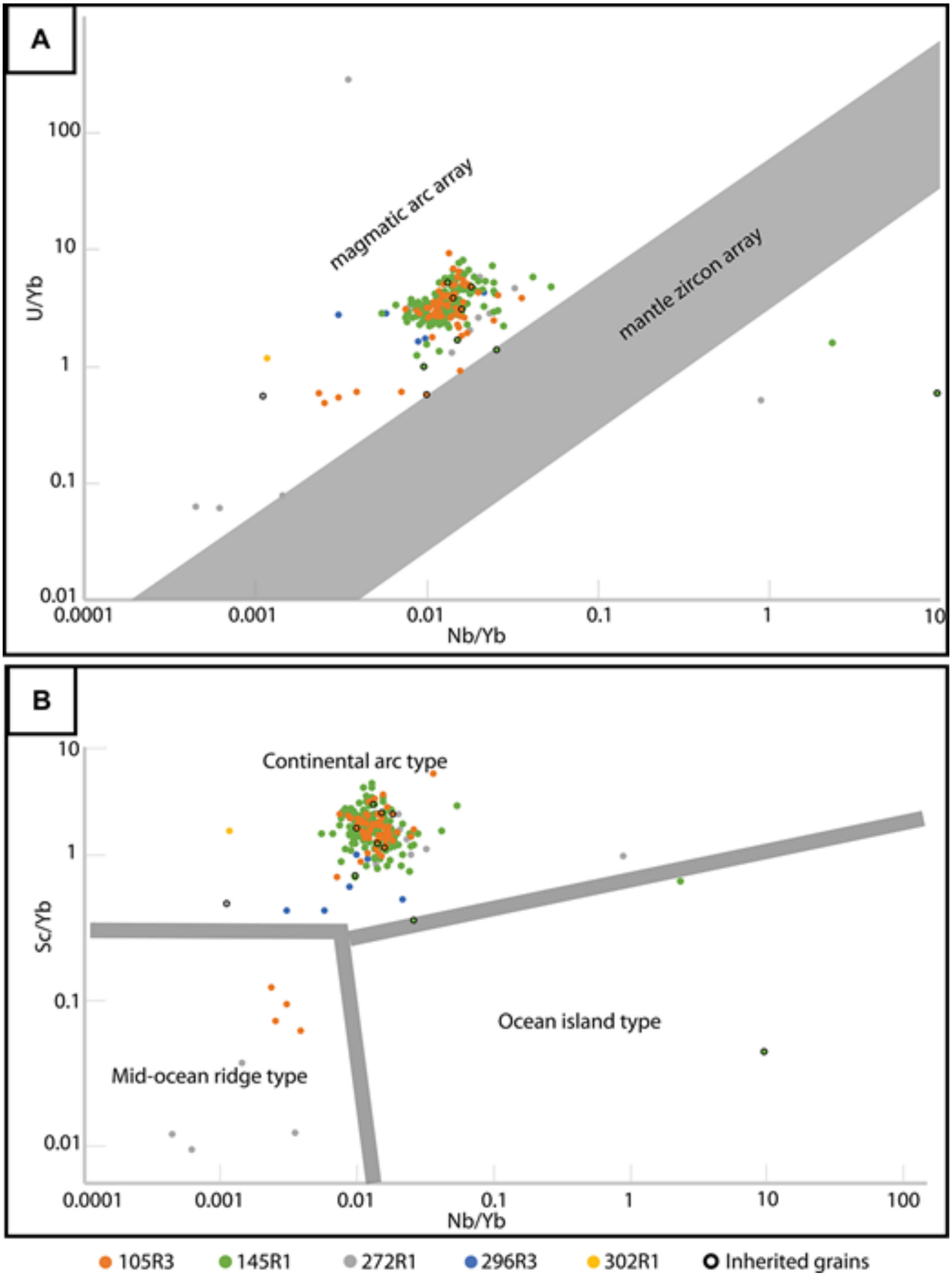
A
magmatic arc array
mantle zircon array
U/Yb
Nb/Yb
100
10
1
0.1
0.01
0.0001
0.001
0.01
0.1
1
10
B
Continental arc type
Ocean island type
Mid-ocean ridge type
Sc/Yb
Nb/Yb
10
1
0.1
0.01
0.0001
0.001
0.01
0.1
1
10
100
105R3
145R1
272R1
296R3
302R1
Inherited grains

Figure 10. Zircon trace element discrimination plot of five samples is after Grimes et al. (2015). (A) U/Yb versus Nb/Yb; (B) Sc/Yb versus Nb/Yb. Inherited grains (600–500 Ma) are outlined in black.

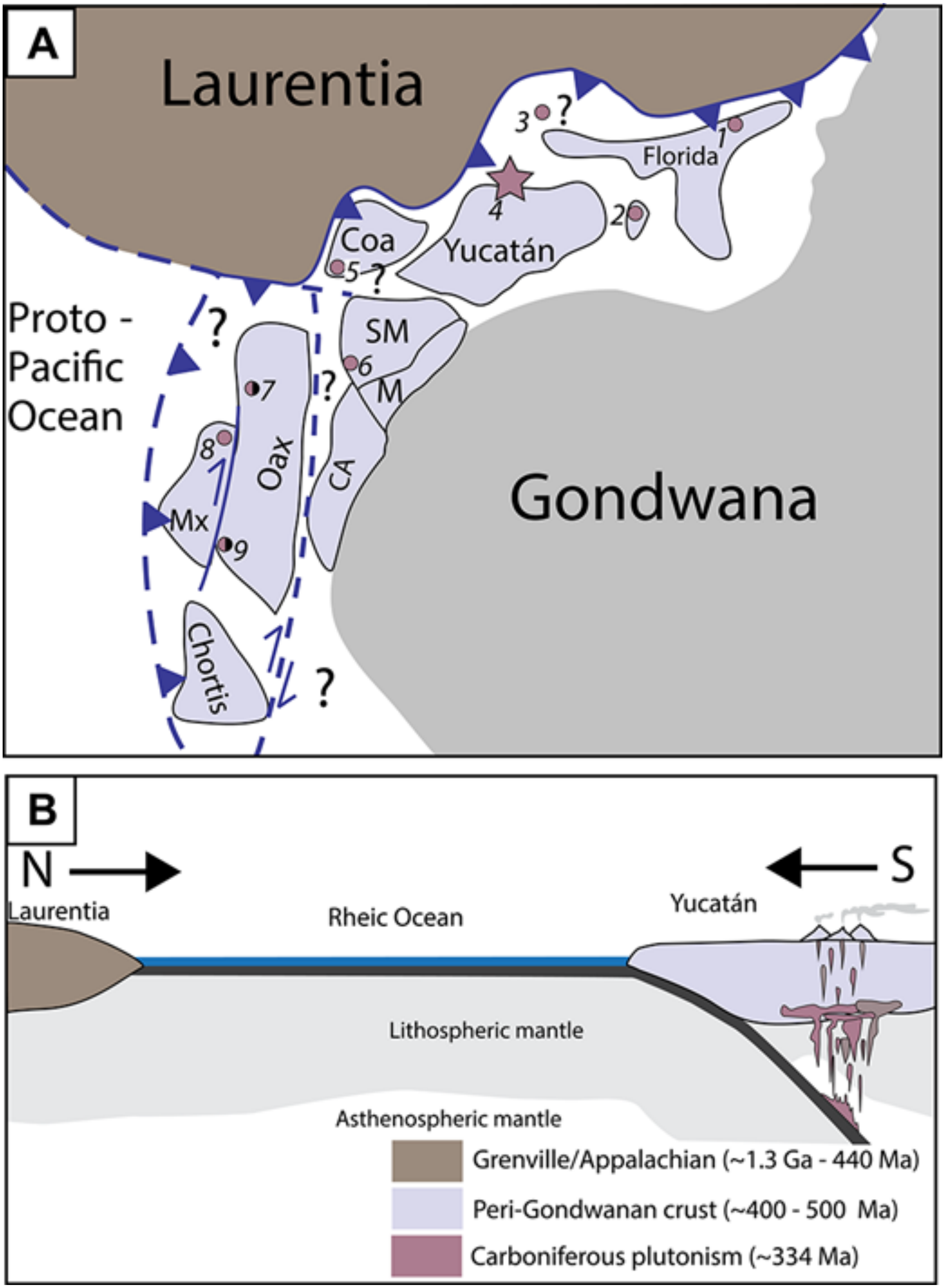
A
Laurentia
Proto - Pacific Ocean
Gondwana
Florida
Yucatán
Coa
SM
M
CA
Oax
Mx
Chortis
1
2
3
4
5
6
7
8
9
?
B
N
S
Laurentia
Rheic Ocean
Yucatán
Lithospheric mantle
Asthenospheric mantle
Grenville/Appalachian (~1.3 Ga - 440 Ma)
Peri-Gondwanan crust (~400 - 500 Ma)
Carboniferous plutonism (~334 Ma)

Figure 11. (A) Tectonic reconstruction of west-central Pangea in the Late Carboniferous-Early Permian is modified from Kirsch et al. (2013). Purple dots represent the reconstructed locations of Carboniferous arc magmatism. Black dots represent locations of Permian arc magmatism. 1—Suwannee terrane granites from wells in South Georgia, Alabama, and Florida (Dallmeyer, 1989a; Mueller et al., 2014); 2—Deep Sea Drilling Project Leg 77 Holes 537 and 538A (Dallmeyer, 1984, 1988); 3—Wiggins Uplift (Dallmeyer, 1989a); 4—International Ocean Discovery Program Expedition 364 (this study); 5—Las Delicias Basin (Lopez, 1997; Lopez et al., 2001; McKee et al., 1999); 6—Atlos Cuchumatanes (Solari et al., 2009, 2010); 7—El Aserradero Rhyolite (Stewart et al., 1999); 8—Totoltepec pluton (Kirsch et al., 2013); 9—Cuanana Pluton and Honduras batholith (Ortega-Obregón et al., 2014). AC—Acatlan Complex (Mixteca terrane); CA—Colombian Andes; Cho—Chortis Block; Coa—Coahuila; M—Merida terrane; Oax—Oaxaquia; SM—Southern Maya (proto-Chiapas Massif Complex). (B) Schematic cross-section from across west-central Pangea. North-south closure of the Rheic Ocean between southern Laurentia (present-day Texas and Louisiana) and the Yucatán. Laurentia (brown) is dominated by Grenvillian-aged crust (1–1.3 Ga) and Appalachian crust (490–440 Ma, 420–350 Ma, and 330–270 Ma). Yucatán (purple) is dominated by Peri-Gondwanan crust (500–400 Ma). Plutonism dated within the Chicxulub crater in this study is shown in purple.

TABLES

Table 1: Sample weighted mean ages from Hole M0077A

				30% discordance filter		15% discordance filter					5% discordance filter				
Sample	Interval top (cm)	Interval bottom (cm)	Approx depth (mbsf)	Grains analyzed	30% filter (exl. Inherited grains)	Grains passed 15% disc. filter	Age (Ma)	Uncertainty (95% confidence interval)	MSWD	Std. deviation	Grains passed 5% disc. filter	Age (Ma)	Uncertainty (95% confidence interval)	MSWD	Std. deviation
104R3	30	35	770	2	2	2	323.9	25.8	71.5	18.6	1				
105R3	33	43	772	91	83	71	325.9	4.8	55.2	20.7	55	330	5.1	46	19.1
106R2	62	67	775	9	9	9	309.9	17.2	84.4	26.4	8	311.4	17.1	88.1	24.7
107R3	0	5	780	25	21	20	313.5	8	17.1	18.2	17	316.4	4.3	9.4	9
121R2	23	33	812	71	55	41	324.8	3.7	14.6	12	24	324.2	4.7	14	11.8
123R1	10	15	820	65	62	51	329.9	3.9	45.8	14.1	36	333.8	3.9	30.7	11.9
145R1	34	44	875	245	119	62	334.7	4	29.1	16	16	344	6.8	24.4	13.9
155R1	45	50	897	19	15	10	327.3	14.3	14.2	23	8	328.6	6.2	12.5	8.9
157R1	60	65	903	24	24	21	314.5	6.8	17.6	16	20	315.3	5.3	16.9	12.1
158R1	98	108	907	6	6	6	316.4	8	17.1	10	5	320.9	7.4	6.3	8.5
183R2	20	25	970	75	65	51	336.5	4.3	49.4	15.8	25	342.2	5.6	37.5	14.3
184R2	48	53	973	71	63	58	337.1	3.8	46.4	14.7	43	339.3	4.6	39.7	15.4
209R2	50	55	1045	6	4	3	338.2	21.3	45.3	18.9	2	319.3	22.9	51	16.5
212R2	10	15	1055	22	18	14	320.4	8.7	11.5	16.7	10	328.4	11.6	39.8	18.7
224R1	0.5	10.5	1090	9	7	7	313.1	14.3	57.5	19.3	3	328.5	14	26.4	12.4
235R3	58	63	1123	16	14	S	324.5	3.3	3.7	6	9	326	3	1.1	4.6
260R2	20	25	1200	28	24	21	320.4	7	18.7	16.4	19	321.3	6.6	15.7	14.6

261R2	0	5	1203	33	31	30	321.2	5.1	21.1	14.3	29	321.3	5	21.6	13.8
272R1	59	69	1237	18	14	14	322	10.8	54.2	20.6	7	328.8	6.4	7	8.6
296R3	16	26	1310	7	3	2	317.3	17.6	41.5	12.7	1				
302R1	20	25	1330	4	2	2	310.8	8.4	5.2	6.1					
Note: MSWD—mean square of weighted deviates; mbsf—meters below seafloor															